Mathematics

AIMS Mathematics, 11(6): 19242–19285.
DOI: 10.3934/math.2026783
Received: 04 May 2026
Revised: 10 June 2026
Accepted: 17 June 2026
Published: 30 June 2026

https://www.aimspress.com/journal/Math

Research article

Adaptive fractional-order moth flame swarm intelligence algorithm for optimal reactive power dispatch and stability enhancement in power grids

Babar Sattar Khan[1], Affaq Qamar[2], Abdul Wadood[3,4,*], Hani Albalawi[3,4], Herie Park[5,6,*], and Byung O Kang[5,*]

[1] Department of Electrical Engineering, COMSATS University Islamabad Attock campus, Pakistan
[2] Department of Electrical Engineering, College of Engineering, Imam Mohammad Ibn Saud Islamic University (IMSIU), Riyadh 12271, Saudi Arabia
[3] Zero Emission Technologies Innovation Center, University of Tabuk, Tabuk 47913, Saudi Arabia
[4] Department of Electrical Engineering, Faculty of Engineering, University of Tabuk, Tabuk 47913, Saudi Arabia
[5] Department of Electrical Engineering, Dong-A University, Busan 49315, Republic of Korea
[6] Department of ICT Integrated Safe Ocean Smart Cities Engineering, Dong-A University, Busan 49315, Republic of Korea

* **Correspondence:** Email: wadood@ut.edu.sa, bakery@donga.ac.kr, bokang@dau.ac.kr.

Abstract: This paper presents a fractional-order swarm intelligence optimization framework for solving the optimal reactive power dispatch (ORPD) problem in modern power grids. The proposed method integrates fractional calculus into the moth-flame optimization algorithm to capture the memory and hereditary characteristics inherent in complex power systems. The fractional-order formulation enhances information exchange among candidate solutions and improves the exploitation capability of the search process. The resulting fractional-order moth-flame optimization (FMFO) algorithm was applied to IEEE benchmark power systems to minimize real power losses and voltage deviations while considering flexible alternating current transmission system (FACTS) device constraints. Simulation results demonstrate significant performance improvements, achieving active power loss reductions of 17.53% in the IEEE-30 bus system, 43.32% in the modified IEEE-30 bus network, and 22.5% in the IEEE-57 bus system. Furthermore, voltage deviation was reduced by up to 84% in the IEEE-57 benchmark system. Statistical evaluations confirm the robustness, stability, and

superior convergence behavior of the proposed fractional-order swarm optimization framework compared with conventional optimization techniques, demonstrating its effectiveness for intelligent power system operation.

Keywords: fractional calculus; moth flame optimization; real power losses; voltage deviations; evolutionary computing
Mathematics Subject Classification: 90C59, 90C30, 34A08, 68T20

1. Introduction

The scientific community engaged in power industries has been increasingly active in addressing optimal power flow (OPF) problems. The implementation of OPF in increasing the efficiency of modern power systems has evolved to become more popular due to several technological, social, and economic advantages. OPF has enhanced the efficiency and controllability of generation, transmission and distribution systems. It also supports the development of fault-tolerant, self-healing, and intelligent energy networks. Although conventional approaches remain prevalent in the power sector, contemporary optimization techniques are crucial for efficiently addressing OPF-related challenges. Optimization approaches give more precise outcomes compared to conventional approaches and offer mathematical formulations that can resolve numerous competing objectives. With the incorporation of innovative flexible alternating current transmission system (FACTS) devices and renewable energy sources (RES), maintaining the dependability and stability of the power system has become an exceedingly difficult task, making optimization strategies an extremely vital component of modern power systems. The primary goals of these optimization challenges are to sustain voltages at suitable levels, reduce losses in power transmission, and lower operating expenses. Optimizing power systems is a complex task due to the presence of numerous local fluctuations, intricate network structures, and the impact of unforeseen events. With the progression of OPF investigations, several techniques have been established or are still being devised to address associated issues. Traditional numerical techniques often fall short in addressing constrained optimization problems within OPF due to the rigid nature of real-world operational limits, frequently resulting in solutions that are entombed in local optima rather than achieving a global optimum. In contrast, stochastic and population-based computational methods have proven more effective in handling the nonlinear, discontinuous, and nonconvex characteristics. As power systems continue to evolve, meta-heuristic algorithms have gained prominence for their ability to solve diverse optimization problems across engineering disciplines with greater accuracy and flexibility than deterministic methods. Their effectiveness lies in features such as adaptability, resilience to premature convergence, and freedom from gradient-based requirements. Continuous advancements in this area aim to further enhance their capability to manage the intricate challenges of real-world power system optimization.

Numerous advanced algorithms designed to address optimization challenges in diverse domains have emerged in recent years. Many of these methods have demonstrated strong performance and robustness in finding effective solutions under challenging conditions. Some examples are pareto-based chaotic-enhanced competitive swarm optimizer (CECSO) algorithm [1], epsilon-based multi-objective genetic algorithm (MOGA) [2], augmented multi-objective multi-verse optimizer (AMOMVO) algorithm [3], RIME algorithm [4], and enhanced wombat optimization algorithm (EWOA) [5]. Furthermore, some innovative methodologies have enhanced the diversification and effectiveness of optimization techniques. A non-dominated sorting multi-objective symbiotic organism search (NSMOSOS) algorithm is presented in [6] to produce the ideal feature subset for brain computer interfaces (BCIs). Two data sets based on motor imagery are used to examine the effectiveness and resilience of the suggested algorithm as a feature selection technique. For datasets 1 and 2, NSMOSOS achieved the greatest classification accuracy of 97.86% with 11 features and 96.57% with an average of 19 features, respectively. The multi-objective generalized normal distribution optimization (MOGNDO) algorithm, which is an improvement of the generalized normal distribution optimization (GNDO) algorithm and has been modified for multi-objective optimization tasks in [7]. Two essential characteristics for multi-objective optimization have been added to the GNDO method, which was previously well-known for its efficacy in single-objective optimization. To ensure a thorough record of the best results, the first is the addition of an archiving mechanism to store non-dominated pareto optimal solutions. A new leader selection system, which is intended to strategically find and choose the finest solutions from the archive to direct the optimization process, is the second improvement. This improvement establishes MOGNDO as a state-of-the-art multi-objective optimization system and establishes a new standard for comparing its performance to industry leaders. A unique multi-objective water strider algorithm (MOWSA) is developed [8] for a variety of difficult physical world structure optimization design problems, and its non-dominated sorting (NDS) framework was investigated. recent ideas for the water strider algorithm, a population-based mathematical paradigm centered on the lifespan of water strider insects, served as the impetus for this endeavor. To enhance the exploration and exploitation trade-off behavior as the quest progresses, MOWSA incorporates the crowding distance feature. Additionally, the proposed method uses the NDS technique to preserve population diversity, which is important for meta-heuristics, particularly for multi-objective optimization. The study in [9] discusses the difficulties in managing OPF in hybrid power systems that use a variety of energy sources, with a special emphasis on the unpredictability of RES. Using multi-objective thermal exchange optimization (MOTEO), a new analytics method is presented. Newton's law of cooling serves as the foundation for MOTEO's modelling of energy transfer. The model successfully solves the multi-objective optimization problem by combining creative non-dominated sorting and crowing distance algorithms. The suggested hybrid OPF model offers a comprehensive approach to power management in hybrid systems by incorporating the four main categories of energy resources: thermal, wind, solar, and small-hydro. The multi-objective marine-predator algorithm (MOMPA), a novel multi-objective algorithm based on elitist non-dominated sorting and crowding distance mechanisms, is proposed in the paper in [10]. Inspired by biological interactions between predators and prey, the suggested method is based on the newly proposed marine-predator method. When tackling optimization problems, the suggested MOMPA can handle several competing objectives. Elitist non-dominated sorting and crowding distance methods are used to formulate the MOMPA.

A novel multi-objective equilibrium optimizer (MOEO) is presented in [11] to address challenging optimization problems, such as practical engineering design optimization problems. The models used to anticipate equilibrium state and dynamic state served as the inspiration for the equilibrium optimizer (EO), a recently published physics-based metaheuristic algorithm. By integrating models in a different target search area, MOEO uses a similar process. The MOEO algorithm uses the crowding distance mechanism to balance the stages of exploration and exploitation as the search moves forward. To maintain population diversity, a non-dominated sorting strategy is also used with the MOEO algorithm. This has been seen as a critical issue in multi-objective metaheuristic algorithms.

There is no research in the literature to create a multi-objective version of the grey wolf optimizer (GWO) due to its uniqueness. For the first time, a multi-objective grey wolf optimizer (MOGWO) was proposed to optimize problems with multiple objectives [12]. The GWO incorporates a fixed-sized external archive to store and retrieve the pareto optimum solutions. The social order and the hunting behavior of grey wolves in multi-objective search spaces are then defined using this repository. The suggested approach was evaluated on 10 multi-objective benchmark problems and contrasted with 2 popular meta-heuristics: multi-objective particle swarm optimization (MOPSO) and multi-objective evolutionary algorithm based on decomposition (MOEA/D). By incorporating both generating cost and emissions as objectives and considering sophisticated limitations like ramp-rate limits, prohibited operating zones (POZs), and valve-point effects (VPE), the study in [13] offers a unique method. A hybrid shuffled frog leaping algorithm (SFLA) and PSO are used to solve the multi-area dynamic economic load dispatch (MADELD) problem, which is further improved by demand response programs (DRP). This approach outperforms conventional single-objective approaches by offering a more solid, effective, and dependable solution that tackles problems related to the economy, environment, and system dependability. A novel low-carbon scheduling model that minimizes operating costs, lowers voltage deviations, and includes a tiered carbon emission trading (CET) mechanism is proposed in [14]. Additionally, a dynamic reactive power optimization technique based on tiered operating costs is proposed to meet limitations on the number of discrete device activities during the scheduling period. The optimal active-reactive power dispatch problem (OARPD) problem with renewable generators was then solved using an enhanced multi-objective equilibrium optimizer (IMOEO).

A recently developed ant-lion optimizer (ALO) is used in [15] to address the power system's ORPD problem. Typically developed as OPF, the ORPD is a volt-ampere reactance (VAR) planning problem that is a highly nonlinear, nonconvex, and difficult optimization problem. Additionally, this article suggests enhancing ALO's search capabilities. To enhance the algorithm's exploration property, a new weighted elitism idea is implemented during the elitism phase of the original ALO. By cleverly balancing exploration and exploitation, the suggested modified ALO (MALO) improves ALO's hunting capabilities. A suggested method for solving the optimum reactive power management (ORPM) problem based on a multi-objective function utilizing a modified differential evolution algorithm (MDEA) is presented in [16]. By resolving the ORPM issue, the suggested MDEA is examined to improve the voltage profile and lower the active power losses. Considering the limitations of the system, the ORPM objective function seeks to reduce transmission power losses and voltage deviations. By updating the self-adaptive scaling factor, which may dynamically exchange information with every generation, the MDEA seeks to improve the differential evolution algorithm's convergence characteristic. To effectively remove entrapment in local optima, the scaling factor dynamically adapts the global and local searches. Furthermore, a method is created to modify the penalty factor to mitigate the impact of different system limitations. An optimization approach based on the gravitational search algorithm (GSA) is used in [17] to determine the best distribution of FACTS devices in the gearbox system. IEEE 30 and IEEE 57 test bus systems are considered benchmarks. The power system's active and reactive loads is considered, and the impact of FACTS devices on each generator's power transfer capacity is examined. The suggested method of using FACTS devices to plan reactive power sources is compared with other widely recognized methods such as PSO, genetic algorithm (GA), and differential evolution (DE). According to the results, the power system's load increases significantly when FACTS devices are added, and each generator in the system can dispatch a sizable amount of active power under various increasing loading conditions while maintaining a steam flow rate that corresponds to the base active loading condition. The work conducted in [18] utilizes FVSI method to detect the weak bus. GWO-PSO is proposed in [18] for providing the optimal solution to the RPP problem. For evaluating the effectiveness of the proposed approach, a comparison is made between

PSO and GWO-PSO approaches. The optimal result obtained through the proposed approach is compared to other heuristic algorithms. The developed algorithm of GWO-PSO reduces the operational costs by 4.25% in the case of IEEE 30 bus system and 5.99% in the case of New England 39 bus system.

To address the shortcomings of the traditional snake optimizer, such as slow convergence, poor solution accuracy, and vulnerability to local optima in complex optimization problems, the study in [19] presents a multi-strategy improved snake optimizer (MISO) and applies it to library robot path planning. First, the population is initialized via tent mapping, which also increases variety and unpredictability and improves global optimization capabilities. Second, to balance local exploitation and global search, a dynamic inertia weight factor is paired with Lévy flight to maximize search performance during the exploration phase. Third, individual positions are updated and diversity is maintained via the use of centroid opposition-based learning. The CEC 2005 benchmark test function set was used to assess MISO's performance. The findings demonstrate that, on the majority of the 23 test functions, MISO beats 10 comparison methods. Although the sparrow search algorithm (SSA) is a revolutionary swarm intelligence technique, it suffers from issues including poor stability, low solution accuracy, and inadequate convergence speed. In order to overcome these drawbacks, we suggest an improved SSA that incorporates the WOA, which creatively combines three improvement strategies [20]: (1) an initialization strategy based on chaotic mapping and opposition-based learning is used to increase the diversity of the initial population; (2) a spiral updating strategy based on the novel inverted S-shaped inertia weight is used to balance the global exploration and local exploitation capabilities of ESSA; thereby improving the convergence speed, accuracy, and stability of ESSA, and (3) to prevent ESSA from prematurely converging, the global optimum solution is perturbed using a position mutation technique based on double random numbers. Comprehensive numerical experiments using 12 state-of-the-art optimization algorithms on CEC2017 and CEC2022 confirmed the superiority and competitiveness of ESSA. The study in [21] suggests a median-driven whale optimization algorithm (MWOA) for feature selection with an emphasis on examining students' reading habits to address the shortcomings of the original whale optimization algorithm (WOA), such as inadequate population diversity, a poor balance between exploration and exploitation, and susceptibility to local optima. MWOA incorporates four major enhanced tactics: the basic population's variety is increased using tent chaotic mapping, and global exploration and local exploitation are dynamically balanced by the nonlinear convergence factor. To increase local search and global efficiency, the position update technique based on the median splits the population into two groups and uses Gaussian mutation and Cauchy mutation, respectively. To prevent local optima, the differential mutation method based on the median optimizes the best solution for the present generation. MWOA outperforms 10 cutting-edge optimization algorithms in terms of convergence speed, solution correctness, and stability when tested on 30-D CEC2017, 50-D CEC2017, 10-D CEC2022, and 20-D CEC2022 benchmark functions.

Power system specialists are continuously investigating innovative optimization techniques for techno-economic plans to provide a secure and reliable energy market. The article in [22] presents a detector for power theft leveraging smart meter data via extreme gradient boosting (XGBoost) algorithm. Measured data undergoes preprocessing, which includes the recovery of misplaced and erroneous values, as well as standardization. The XGBoost-based classification model undergoes training on both normal and malicious data. In comparison to other machine learning techniques, the suggested approach demonstrates superior accuracy or a reduced false-positive rate in detecting energy theft. The research in [23] presents a distributed optimization approach for a hybrid microgrid network aimed at minimizing overall generation costs in a dynamic economic dispatch (DEDP). The integrated micro-grid system is comprised of several conventional power sources, RES, and energy battery storage. All of these power sources are governed by supply-demand equilibrium, capability limitations, and ramp-rate constraints of generating sources. Meanwhile, from the standpoint of environmental protection, pollutants released from conventional generators are deemed to mitigate their environmental effect. Ultimately, simulations of experiments using quadratic and non-quadratic cost functions, together with comparative examples, demonstrate that the ideal solution adheres to the supply-demand restraints as well as capability disparities at each time interval. Power system contains several voltage-regulating devices, such as tap-changing transformers [24], synchronous condensers [25], TCSC, and static VAR compensator [26]. Nevertheless, the optimum positioning of FACTS devices and the setting of control variables presents a complex constraint optimization task. This advancement significantly impacts system stability by reducing real power losses, improving voltage profiles, increasing network load capacity, enhancing voltage stability, and reducing fuel costs [27,28]. Nodal analysis indicates the presence of weak buses for the use of FACTS devices [29]. The adoption of energy from RES is progressively rising due to its benefits in addressing current difficulties, such as the growing need for electricity [30]. Microgrids have garnered significant interest owing to their numerous advantages. Microgrids can effectively provide electricity to rural and vulnerable regions while enhancing system resilience. Like other systems, microgrids need a dependable control system to ensure optimal functionality. Control techniques include robust control and adaptable control, while control structures may be categorized into two types: centralized and decentralized. The study in [31] presents an overview of several decentralized control methodologies for microgrids. The methodologies used in each investigation are comprehensively detailed, along with their outcomes. Additionally, other research enquiries have been proposed for future investigation concepts of zero - carbon clean energy, like hydrogen, are being swiftly developed to minimize carbon emissions, encouraging their use as the primary energy source for multi-energy micro-grids (MEMGs). The fundamental challenge of the MEMG scheduling issue is handling source/load uncertainty to ensure solution viability and economics in operation. To achieve this, the multi-stage adaptive stochastic robust optimization (MASRO) technique that combines robust optimization with stochastic programming has been proposed.

Considering the rising prevalence of distributed generators (DGs) and the escalating need for the dependable energy sources, it is essential to swiftly detect abnormalities in active distribution networks (ADNs) [32]. Moreover, abnormality detection is essential for directing maintenance actions to address issues after the activation of relay protection. The article in [32] describes a fast and accurate ADN anomaly detection method. The suggested technique comprises three levels of tightly coupled modules. Initial data is processed by an iterative clustering layer in the first module. The second module looks for hidden patterns based on anomalies and post-fault voltage using an association rule layer. The third module trains accurate identification models using regression training. The case study uses IEEE 33-bus system data with dispersed generations and actual distribution network post-fault data. Comparative experiments show that the suggested data-mining structure may be used in the ADN state awareness system due to its high recognition accuracy and quick response times. In hybrid networked micro-grids with three-phase AC/DC, a heuristic rule-based distributed power flow algorithms may have convergence problems when processing limits [33]. This research developed a completely distributed power flow (DPF) calculating approach that can reliably manage converter reactive power constraints and step voltage regulator voltage control without excessive model dependency on the initial parameters. Authors in [34] proposed a more efficient and dependable evolutionary-based method for resolving the ORPD problem. The suggested methodology utilizes a DE algorithm to identify the most appropriate values for the control variables of the ORPD problem. The simulation outcomes of the suggested technique are compared to the findings documented in the literature. The statistics clearly illustrate the efficacy and long-lasting nature of the suggested strategy in resolving the ORPD problem. To address the issue of premature convergence in PSO, a learning technique known as comprehensive learning particle swarm optimization (CLPSO) was proposed [35]. The research investigated three unique test cases. The findings of the research show that the approaches mentioned above are viable and effective. In [36], harmony search algorithm (HSA) was used to solve the ORPD problem. The methodology proposed will optimize tap settings of transformers, reactive compensators, and generator voltages.

Hybrid approaches are more rigorous than their component methods when used individually and therefore converge on optimum solutions more quickly. The best solutions are ensured by the hybridization techniques, owing to the fact that these techniques make use of the best features of each technique. Combining multiple search algorithms sanctions an in-depth investigation within the solution space by balancing exploration and exploitation strategies. In earlier research in power systems, many hybrid strategies have been actively implemented. The primary motivation to conduct a thorough literature study in the power systems domain is the increasing prevalence of these techniques. A robust and efficient approach, using a combination of modified imperialist competitive algorithm (MICA) and invasive weed optimization (IWO) techniques, was introduced to address the ORPD problems [37]. The ICA algorithm often converges towards local optima. To address this limitation, a novel approach is suggested that leverages the benefits of the IWO method to enhance the local search around the global best solution. Additionally, a set of modifications is proposed for the assimilation strategy rule of the ICA to further improve the algorithm's convergence rate and achieve higher solution quality. The hybrid MICA-IWO approach is subsequently proposed for addressing the ORPD problem. An innovative teaching learning-based optimization (TLBO) method was introduced in [38] as a means of resolving the multi-objective ORPD problem. To optimize the solution and accelerate the convergence process, the quasi-opposition-based learning (QOBL) was assimilated into the initial TLBO algorithm. The outcomes unequivocally demonstrate that the proposed quasi-oppositional teaching learning-based optimization (QOTLBO) strategy surpasses both the initial TLBO and alternative optimization strategies. This substantiates its capacity to efficiently tackle ORPD concerns. The study in [39] introduces a new approach that combines entropy evolution (EE) and fractional calculus (FC) principles. The innovative entropy moth flame optimization fractional - order PSO (EMFO-FPSO) is tested utilizing the standard 57 and 118 IEEE bus systems. The suggested EMFO-FPSO method has been shown to be superior by comparative analysis research with established optimizer algorithms from literature.

A novel, nature-inspired computer paradigm has been created and used to solve the ORPD problem. This paradigm has been successfully used and is based on fractional-order comprehensive learning particle swarm optimization (FO-CLPSO) [40]. To achieve multiple objectives in ORPD, the use and exploration of FO-CLPSO are extended via the use of different fractional orders. This is carried out in detail to assess efficacy via comparison with a variety of cutting-edge methods. Comprehensive statistical studies demonstrate the reliability, consistency, robustness, and dependability of FO-CLPSO in handling ORPD problems. In the study presented in [41], the authors have used swarm intelligence algorithms to efficiently coordinate FACTS devices with other reactive power compensation devices in the power system. The study reported in [42] utilizes DE, GA optimization approaches in combination with fuzzy Logic to determine the best configuration of variables, incorporating FACTS devices. Two kinds of FACTS devices, namely TCSC and SVC, are used to ensure the efficient functioning of the power system and alleviate bottlenecks in transmission lines. In order to tackle the OPF problem, the study in [43] presents the artificial hummingbird algorithm (AHA), which has been enhanced for convergence and solution accuracy by combining it with QOBL algorithm. When tested on the IEEE 57-bus system, the suggested quasi-oppositional artificial hummingbird algorithm

(QOAHA) outperforms current optimization methods in terms of cost and emission reduction. The statistical analysis and benchmark functions enable the proposed method to resolve the ORPD problem. The authors in [44] have presented the voltage collapse proximity index (VCPI) approach, which utilizes oppositional Harris hawks optimization (OHHO) to find weak branches. The recommended scheme is used to resolve the ORPD problem on two test systems: the Ward Hale 6 bus test system and the modified IEEE 30 bus test system. The suggested methodology is evaluated against many contemporary optimization strategies. The OHHO technique demonstrates favorable outcomes for uncompensated systems. The cuckoo search method and ALO are used to determine the optimum location of TCSC [45]. The results indicated a significant decrease in both reactive and actual power losses, as well as voltage variations under normal and overloaded operating circumstances. The restoration of power flow security is achieved after the occurrence of overloading circumstances by using the TCSC. The article in [46] suggests combining the OMPA with HHO algorithms to create a novel technique called OMPA-HHO. The strategy in search space is hybridized and mutated by merging marine predator algorithm (MPA) with the oppositional based learning (OBL) approach. This leads to enhanced assessment for the dominant solution. The suggested approach has been validated by compiling it on 23 standard benchmarking operations. Reactive power projection is a challenging matter for engineers. The outcomes of the simulation show enhanced performance. The findings confirm the capacity of the OMPA-HHO to scale, repeat, and withstand challenges, improving it for solving complicated optimization problems. Enhanced Jaya and artificial ecosystem-based optimization (EJAEO) is a hybrid algorithm that is suggested in [47] as a solution to the ORPD problem. To determine the optimal parameter values like reactive compensation, generator voltages, and transformer tap ratio, the algorithm is designed. Comparing the EJAEO algorithm against three other recent algorithms, namely artificial ecosystem-based optimization (AEO), turbulent flow of water-based optimization, and Jaya algorithm, and other previously published ORPD techniques, the simulation findings indicated that the EJAEO algorithm performed better in terms of convergence. The reactive power optimization challenge tackled by the HHO method has sluggish convergence and local optima stagnation [48]. In addition, the application of the approach to reactive power optimization results in significant reduction of 33.19% in active power loss, which guarantees the security of the system. The experimental assessment of benchmark functions reveals improved performance. The research work in [49] presents a novel hybrid method that integrates the MFO and PSO techniques for the purpose of estimating transmission line characteristics. The hybrid strategy exhibits enhanced performance regarding both convergence rate and quality of the solution when compared to traditional PSO and MFO methodologies. This enhancement in efficiency contributes to the improvement of parameter estimation in power systems.

In recent years, integrating fractional-order swarming techniques into the core structure of optimization algorithms has been actively explored [50,51]. Such methods have been effectively applied in various areas, including the analysis of power system optimization [52], edge server allocation [53], power system protection [54], photovoltaic power prediction [55], UAV swarm formation [56] and parameter extraction of photovoltaics model [57]. The combination of an evolutionary strategy with a fractional calculus-based technique has been found to provide a viable way for solving optimization problems in the energy industry. The researchers of this study were motivated by a hybridization technique that combines many meta-heuristic algorithms for achieving a balanced equilibrium between exploitation and exploration.

Digitalization is making power grids more significant, but that means we need to maintain reliable operation under external faults, communication constraints, and cyberattacks. Recent research studies shows that networked control systems work effectively through coordinated use of anti-disturbance and attack-resilient controls. These systems cut down on extra data sharing and maintain good control performance [58]. Moreover, augmented observers enable real-time estimation and compensate for unknown disturbances in real-time. These developments provide a valuable theoretical foundation for improving the practical applicability of optimization-based power system control approaches. Even though the FMFO algorithm is made for steady-state ORPD and lacks cyber-resilient controls, its strong optimization skills still make it a great complementary decision-making tool. Combining FMFO with event-triggered anti-disturbance and attack-tolerant controls could boost security, resilience, and efficiency in real smart grids, making them more dependable and effective against renewable energy uncertainties, communication constraints, load fluctuations and cyber-attacks. So, extending the FMFO method for more resilient power networks seems like a great area to explore further in future research.

This study examines an innovative methodology through a hybrid computation framework of FC and MFO algorithms as the FMFO algorithm for ORPD implementation involving the integration of FACTS in electrical power networks. In order to ensure that global optimum results are achieved, the computation technique of FMFO algorithm is employed to attain effective searching abilities. Key points are summarized as follows:

- Application of the FMFO algorithm aims to reduce real power losses and voltage deviations through meeting load demands and adhering to system constraints.
- An analysis of FMFO's effectiveness in ORPD problems is carried out by varying the fractional order.
- Using FACTS devices with FMFO optimization in a novel way to perform the fractional- orders warming method, which yields a reliable solution to ORPD.
- The suggested algorithm's consistency, robustness, and stability are displayed graphically via probability plots, histograms, and boxplots.

This paper is structured as follows: The section titled "System Mathematical Model" outlines the objective functions for ORPD. The "Modeling and design approach" section offers a detailed explanation of the proposed FMFO algorithm. Simulation outcomes and comparative evaluations with existing techniques are thoroughly discussed in the "Simulation Results" and "Statistical Analysis" sections. Finally, the "Conclusion and Recommendations" section summarizes the main findings and offers recommendations for future work.

2. System mathematical model

2.1. Real power losses minimization

Optimal power flow methods estimate real power losses, which depend on voltage magnitudes and phase angles across transmission lines [59] as expressed in Eq (2.1)

$$Min: F(x_1, x_2) = \sum_{r=1}^{N_T} G_r\,[V_a^2 + V_b^2 - 2V_aV_b\cos(\delta_a - \delta_b)]. \tag{2.1}$$

Reducing actual power losses is the objective function's goal and involves two sets of variables: x_1 (dependent variables like generator reactive power, load voltages, and line loadings) and x_2 (controlled variables like generator voltages, transformer settings, VAR compensators, and FACTS devices like SVCs and TCSCs). N_T represents the quantity of transmission lines, G_r is line conductance, V_a, V_b, and δ_a, δ_b are the voltages and angles at the sending and receiving ends, respectively.

The power balance constraints are defined using mathematical expressions, presented in Eqs (2.2) and (2.3)

$$P_{ga} - P_{da} - V_a \sum_{b=1}^{N_{BUS}} V_b (B_{ab}\, sin(\delta_a - \delta_b) + G_{ab}\, cos(\delta_a - \delta_b)) = 0, \quad (2.2)$$

$$Q_{ga} - Q_{da} - V_a \sum_{b=1}^{N_{BUS}} V_b (B_{ab}\, cos(\delta_a - \delta_b) + G_{ab}\, sin(\delta_a - \delta_b)) = 0. \quad (2.3)$$

The representation of active power supply and demand is denoted by P_{ga} and P_{da}, respectively for a^{th} bus. Reactive power supply and demand is represented by Q_{ga} and Q_{da} respectively for a^{th} bus.

Inequality constraints cover generator voltages, reactive power, transformer taps, shunt capacitors, and FACTS limits. Eqs (2.4) and (2.5) define voltage and reactive power bounds for Ng generators, respectively.

$$v_{gn}^{min} \le v_{gn} \le v_{gn}^{max}, \text{ n=1,2, 3, ..., } N_g \quad (2.4)$$

$$Q_{gn}^{min} \le Q_{gn} \le Q_{gn}^{max}, \text{ n=1,2, 3, ..., } N_g \quad (2.5)$$

Eqs (2.6) and (2.7) defines tap settings for transformers and shunt fixed capacitors limits, respectively.

$$T_n^{min} \le T_n \le T_n^{max}, \text{n} = 1,2,3, \dots \dots, \text{NT} \quad (2.6)$$

$$Q_{cn}^{min} \le Q_{cn} \le Q_{cn}^{max}, \text{n} = 1,2,3, \dots \dots, \text{NT} \quad (2.7)$$

TCSC's and SVC's limits are expressed in Eqs (2.8) and (2.9), respectively.

$$TCSC_n^{min} \le TCSC_n \le TCSC_n^{max} \quad \text{n} = 1,2,3, \dots \dots \dots \dots, N_{TCSC} \quad (2.8)$$

$$SVC_n^{min} \le SVC_n \le SVC_n^{max} \quad \text{n} = 1,2,3, \dots \dots \dots \dots, N_{SVC} \quad (2.9)$$

2.2. Mathematical formulation involving FACTS devices

Solid-state devices provide a novel method for managing load flows by minimizing real power losses and voltage deviations while maintaining designated voltage levels. This may be accomplished by incorporating FACTS devices into the electrical power network to control various electrical parameters that include voltages, currents, power angles, active and reactive power flows. In the sub sequent sections, static equivalent models of TCSC and SVC are discussed.

2.2.1. TCSC

The TCSC provides an adjustable reactive impedance jX_{TCSC} that is adjustable both above and below the line of reference impedance. Figure 1 illustrates the static representation of TCSC located between two buses.

The equations governing the active and reactive power flows are provided in Eqs (2.10) and (2.11), respectively, after the TCSC is connected.

$$P_{ab} = +G_{ab}V_a^2 - G_{ab}V_aV_b\,cos(\delta_a - \delta_b) - B_{ab}V_aV_b\,sin(\delta_a - \delta_b), \tag{2.10}$$

$$Q_{ab} = -B_{ab}V_a^2 - G_{ab}V_aV_b\,sin(\delta_a - \delta_b) - B_{ab}V_aV_b\,cos(\delta_a - \delta_b). \tag{2.11}$$

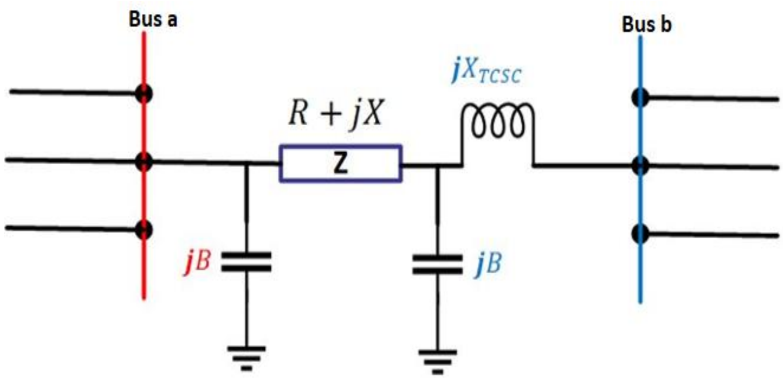

Figure 1. Static illustration of the TCSC equivalent circuit.

Likewise, the flow of active and reactive power from bth bus to ath buses is expressed in Eqs (2.12) and (2.13), respectively.

$$P_{ba} = +G_{ba}V_b^2 - G_{ba}V_bV_a\,cos(\delta_b - \delta_a) - B_{ba}V_bV_a\,sin(\delta_b - \delta_a), \tag{2.12}$$

$$Q_{ba} = -B_{ba}V_b^2 - G_{ba}V_bV_a\,sin(\delta_b - \delta_a) - B_{ba}V_bV_a\,cos(\delta_b - \delta_a). \tag{2.13}$$

2.2.2. SVC

The SVC can be configured to both transmit and receive reactive power. The phase-controlled functioning of a thyristor valve is responsible for regulating the flow of reactive power, which allows for the rapid detachment or addition of capacitors and reactors that are linked in parallel. The comparable SVC paradigm is shown in Figure 2, and it is possible to implement it at each bus. The formula that shows how reactive power is transferred from the SVC to the bus, is presented in Eq (2.14).

$$Q^{SVC} = V^2 * B^{SVC}. \tag{2.14}$$

The FACTS devices in this study are modeled with steady-state operating constraints and practical limits, both min and max, to help the optimal power flow framework. So, they use steady-state rules and set bounds to make optimization easier. Though this modeling approach is widely used for planning and optimization, it does not show detailed dynamic traits like controller time delays, saturation effects, or how FACTS devices work together during changes. Adding these flexible behaviors and advanced multi-device strategies could make power system operations much more realistic and an important direction for future research.

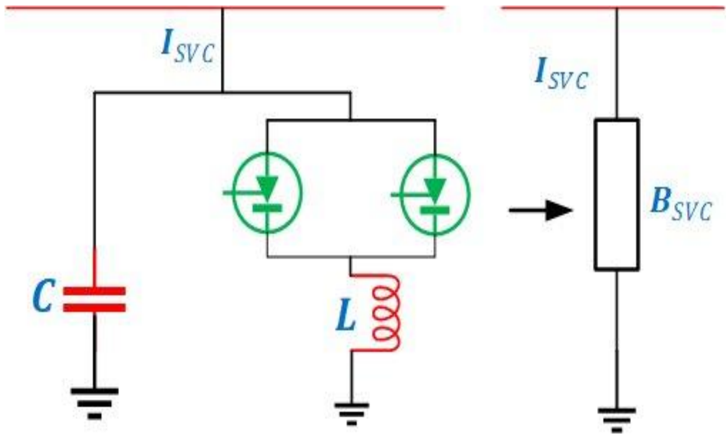

Figure 2. Static illustration of the SVC equivalent circuit.

2.3. Objective function involving voltage deviation minimization

Voltage profile is usually improved to regulate the voltages at load buses of power system. For a more enhanced and efficient performance of power systems, the voltage deviation (V.D) should be as low as possible. With a value of V.D 1 p.u, the voltage profile will be smoother. It is feasible to calculate voltage deviation using the formula expressed in Eq (2.15).

$$Minimize: V.D = \sum_{s=1}^{N_{LB}} [V_s - 1(p.u)]. \quad (2.15)$$

3. Modeling and design approach

This section introduces a new framework referred to as fractional-order moth-flame optimization (FMFO) for enhancing the performance of the conventional MFO algorithm. For classical MFO, moths make use of a spiral search around flames, which helps in exploring the solution space but is prone to early convergence for multimodal problems [60]. To address this problem, fractional driven dynamics are incorporated into our model, making it easier for the moths to manage exploration and exploitation without changing the simplicity of MFO algorithm. Unlike traditional frameworks, the model proposed here does not incorporate any modification in structure within the MFO. It only provides a new definition for the movement process of moths using the fractal velocity process. The modification leads to improvement, which ensure that the movement of the moths is adaptively controlled during the iteration process and facilitates the transition between exploration and exploitation phases. FMFO shows higher adaptability and robustness due to the use of mathematical analogies of the fractal idea of movement instead of a combination of algorithms that preserves the original simplicity of the algorithm.

In the classical version of the MFO algorithm, the position of the ith moth is updated by circling around its corresponding flame in a logarithmic spiral path. The position of each moth around the flame is updated using the *S* spiral function, as shown in Eq (3.1).

$$M_i(\tau+1) = S(M_i(\tau), F_j(\tau)). \tag{3.1}$$

Considering these points, a logarithmic spiral is defined for the MFO algorithm as shown in Eq (3.2).

$$S(M_i(\tau), F_j(\tau)) = D_i(\tau)e^{bt}\cos(2\pi t) + F_j(\tau). \tag{3.2}$$

In this regard, $M_i(\tau)$ and $F_j(\tau)$ represent the positions of the ith moth and jth flame, respectively. $D_i(\tau)$ indicates the distance of the ith moth and the jth flame, b is a constant for defining the shape of the logarithmic spiral, and t is a random number in [−1, 1]. D is calculated in Eq (3.3).

$$D_i(\tau) =\mid F_j(\tau) - M_i(\tau) \mid. \tag{3.3}$$

Though the spiral method offers a good strategy for searching, the classic MFO algorithm does not make use of past search data. Therefore, the motion of each individual moth will depend on its current position relative to the existing source of flame only; the process might result in an early convergence in a highly multimodal environment. The velocity-type state is hence introduced to incorporate memory into the search behavior as defined in Eq (3.4).

$$V_i(\tau) = M_i(\tau) - M_i(\tau-1). \tag{3.4}$$

Using Eq (3.4), the position evolution can be written in Eq (3.5).

$$M_i(\tau+1) = M_i(\tau) + V_i(\tau+1). \tag{3.5}$$

Through the spiral updating mechanism, the displacement required due to the flame attracting phenomenon is given in Eq (3.6).

$$V_i(\tau+1) = D_i(\tau)e^{bt}\cos(2\pi t) + F_j(\tau) - M_i(\tau). \tag{3.6}$$

Eq (2.9) may be compactly represented as in Eqs (3.7) and (3.8).

$$V_i(\tau+1) = G_i(\tau). \tag{3.7}$$

$$G_i(\tau) = D_i(\tau)e^{bt}\cos(2\pi t) + F_j(\tau) - M_i(\tau). \tag{3.8}$$

FC has received considerable attention from multiple scientific fields, resulting in many mathematical models [61]. Of particular note is the Grünwald-Letnikov (GL) approach that is applicable to dynamic systems [62]. Through the GL approach, it becomes possible to further develop theoretical models of the MFO approach, thus providing an enhanced modelling of such complex memory-based systems. Use of the fractional-order operator in the developed optimization methodology is more than a mere numerical transformation; rather, it adds another control process that comes out of fractional-order systems theory. Unlike classical integer-order systems where the future state depends solely on the present state, fractional-order systems are known to have hereditary and memory properties, which allow the present state to be determined by the complete past states. To capture memory effects in the MFO algorithm, the integer-order velocity dynamics of Eq (3.9) is extended via Grünwald-Letnikov fractional differentiation approach. The Grünwald-Letnikov fractional derivative of order α is expressed in Eq (3.10).

$$D^{\alpha} f(t) = \lim_{h \to 0} \frac{1}{h^{\alpha}} \sum_{k=0}^{\infty} (-1)^k \binom{\alpha}{k} f(t - kh), \tag{3.9}$$

$$\binom{\alpha}{k} = \frac{\Gamma(\alpha+1)}{\Gamma(k+1)\Gamma(\alpha-k+1)}. \tag{3.10}$$

Where Eq (3.10) denotes the generalized binomial coefficient, and $\Gamma(\cdot)$is the Gamma function. It can be seen from Eq (3.10) that the present state depends upon all the past states with coefficients depending on the fractional derivative order α. As a result, the path for optimization has the property of long memory, which gives the algorithm an opportunity to keep data about past searches throughout the process. Since the optimization process performed by metaheuristic algorithms is inherently discrete, the sampling period is chosen as

$$h = 1. \tag{3.11}$$

Therefore, Eq (3.9) becomes

$$D^{\alpha} f(\tau) = \sum_{k=0}^{\infty} (-1)^k \binom{\alpha}{k} f(\tau - k). \tag{3.12}$$

Expanding the first few terms of Eq (3.12) yields Eq (3.13).

$$D^{\alpha} f(\tau) = f(\tau) - \alpha f(\tau - 1) + \frac{\alpha(\alpha-1)}{2!} f(\tau - 2) - \frac{\alpha(\alpha-1)(\alpha-2)}{3!} f(\tau - 3) + \cdots \tag{3.13}$$

Applying Eq (3.13) to the moth velocity variable gives Eq (3.14).

$$D^{\alpha} V_i(\tau + 1) = V_i(\tau + 1) - \alpha V_i(\tau) + \frac{\alpha(\alpha-1)}{2} V_i(\tau - 1) - \frac{\alpha(\alpha-1)(\alpha-2)}{6} V_i(\tau - 2) + \cdots \tag{3.14}$$

The fractional-order MFO dynamics are then defined by replacing the integer-order velocity relation of Eq (3.8) with Eq (3.15).

$$D^{\alpha} V_i(\tau + 1) = G_i(\tau). \tag{3.15}$$

Substituting Eq (3.13) into Eq (3.15) yields Eq (3.16).

$$V_i(\tau + 1) - \alpha V_i(\tau) + \frac{\alpha(\alpha-1)}{2} V_i(\tau - 1) - \frac{\alpha(\alpha-1)(\alpha-2)}{6} V_i(\tau - 2) + \cdots = G_i(\tau). \tag{3.16}$$

The order of the velocity derivative can be generalized to a real number $0 \leq \alpha \leq 1$, if the FC perspective is considered, leading to a smoother variation and a longer memory effect. To study the behavior of this new MFO strategy, a set of simulations are carried on testing values of α ranging from α = 0.1 up to α =0.9, with increments of α = 0.1. The influence of fractional order in the optimization process can be understood from the perspective of memory function of the GL operator. As the value of α is smaller, the decay rate for the weight from past experience is lower, so that earlier experiences can continue to have an effect for a longer time. As such, the moth particles maintain higher trajectory diversity and retain their ability to explore globally. Such a feature ensures that premature convergence is avoided, helping the algorithm to escape from local optima. On the contrary, as the value of α tends towards unity, the contribution from distant past state values progressively declines. The fractional operator tends towards a classical difference operator of order one. Considering the first r=4 terms of differential derivative and rearranging Eq (3.16) with respect to the current velocity state results in Eq (3.17).

$$V_i(\tau+1) = G_i(\tau) + \alpha V_i(\tau) - \frac{\alpha(\alpha-1)}{2} V_i(\tau-1) + \frac{\alpha(\alpha-1)(\alpha-2)}{6} V_i(\tau-2) - \frac{\alpha(\alpha-1)(\alpha-2)(\alpha-3)}{24} V_i(\tau-3) + \cdots \tag{3.17}$$

Substituting Eq (3.8) into Eq (3.17) gives the exact infinite-memory fractional velocity update as shown in Eq (3.18).

$$V_i(\tau+1) = D_i(\tau)e^{bt}\cos(2\pi t) + F_j(\tau) - M_i(\tau) + \alpha V_i(\tau) - \frac{\alpha(\alpha-1)}{2} V_i(\tau-1) + \frac{\alpha(\alpha-1)(\alpha-2)}{6} V_i(\tau-2) - \frac{\alpha(\alpha-1)(\alpha-2)(\alpha-3)}{24} V_i(\tau-3) + \cdots \tag{3.18}$$

Equation (3.18) reveals that the current moth movement depends not only on the present spiral guidance term but also on all previous velocity states through a weighted memory structure governed by the fractional order α.

The infinite series from Eq (3.18) is not feasible because memory length needs to increase constantly according to the number of iterations performed. Thus, the finite memory approach is taken into consideration. Retaining the first m terms as shown in Eq (3.19).

$$V_i(\tau+1) = G_i(\tau) + \sum_{k=1}^{m} (-1)^{k+1} \binom{\alpha}{k} V_i(\tau+1-k). \tag{3.19}$$

For $m = 4$, the proposed fractional-order velocity update becomes as shown in Eq (3.20) and is employed in the proposed algorithm.

$$V_i(\tau+1) = D_i(\tau)e^{bt}\cos(2\pi t) + F_j(\tau) - M_i(\tau) + \alpha V_i(\tau) - \frac{\alpha(\alpha-1)}{2} V_i(\tau-1) + \frac{\alpha(\alpha-1)(\alpha-2)}{6} V_i(\tau-2) - \frac{\alpha(\alpha-1)(\alpha-2)(\alpha-3)}{24} V_i(\tau-3). \tag{3.20}$$

The truncation adopted in Eq (3.20) does not neglect the memory effect; rather, it constitutes a finite-memory approximation of the exact Grünwald–Letnikov operator. The contribution of higher-order historical states decreases progressively because of the generalized binomial coefficients as shown in Eq (3.21).

$$c_k = (-1)^k \binom{\alpha}{k}. \tag{3.21}$$

The generalized binomial coefficients decay rapidly with increasing k, for $0 < \alpha < 1$, as shown in Eq (3.22).

$$\lim_{k\to\infty} c_k = 0. \tag{3.22}$$

Thus, the effects of historical velocity states become progressively insignificant. Keeping the first four memory states helps maintain the main properties of the fractional memory process while reducing storage and computation significantly. Therefore, Eq (3.18) provides a practical approximation of the infinite-memory fractional dynamics described by Eq (3.20). The effect of fractional- order dynamics may be further explained using the equivalent transfer function approach as shown in Eq (3.23).

$$G(s) = \frac{1}{s^{\alpha}+a}. \tag{3.23}$$

The corresponding poles are distributed according to Eq (3.24), indicating that the fractional order modifies both damping characteristics and pole locations. Therefore, α acts as a dynamic tuning parameter governing the trade-off between convergence speed and search diversity.

$$s_k = a^{1/\alpha} e^{j\frac{(2k+1)\pi}{\alpha}}, k = 0,1, \ldots \tag{3.24}$$

Therefore, the proposed fractional-order mechanism provides a theoretically grounded approach for balancing global search capability and local refinement. This enhancement is not algorithmic; it arises from the natural stability properties of fractional-order dynamical systems. This forms an explicit link between the theory of fractional calculus and the exploration process of the FMFO algorithm.

Figure 3 illustrates the working mechanism of the proposed FMFO algorithm, while its step-by-step procedure is outlined in Algorithm 1. A graphical overview of the FMFO approach to solve the ORPD problem is presented in Figure 4.

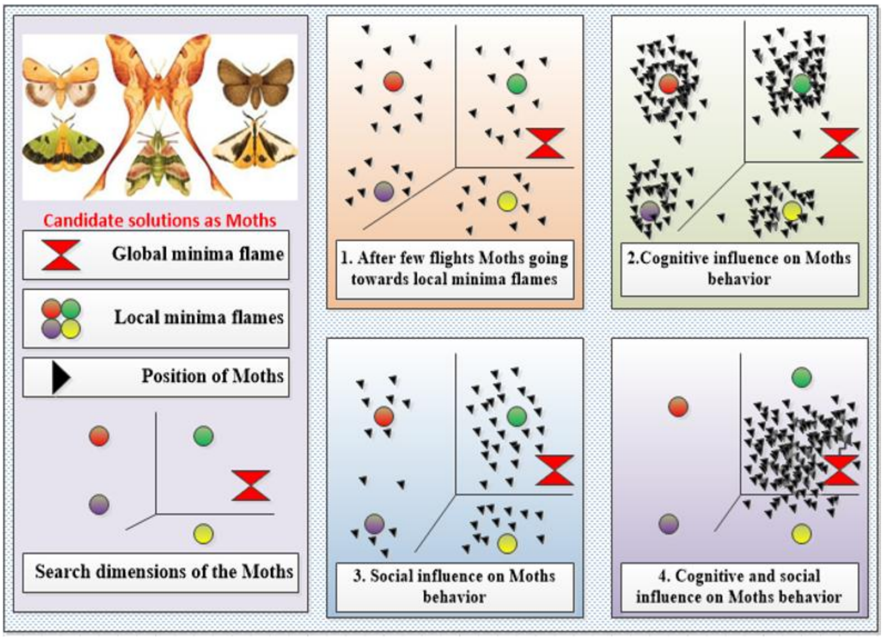

Figure 3. Principle of operation of the FMFO algorithm.

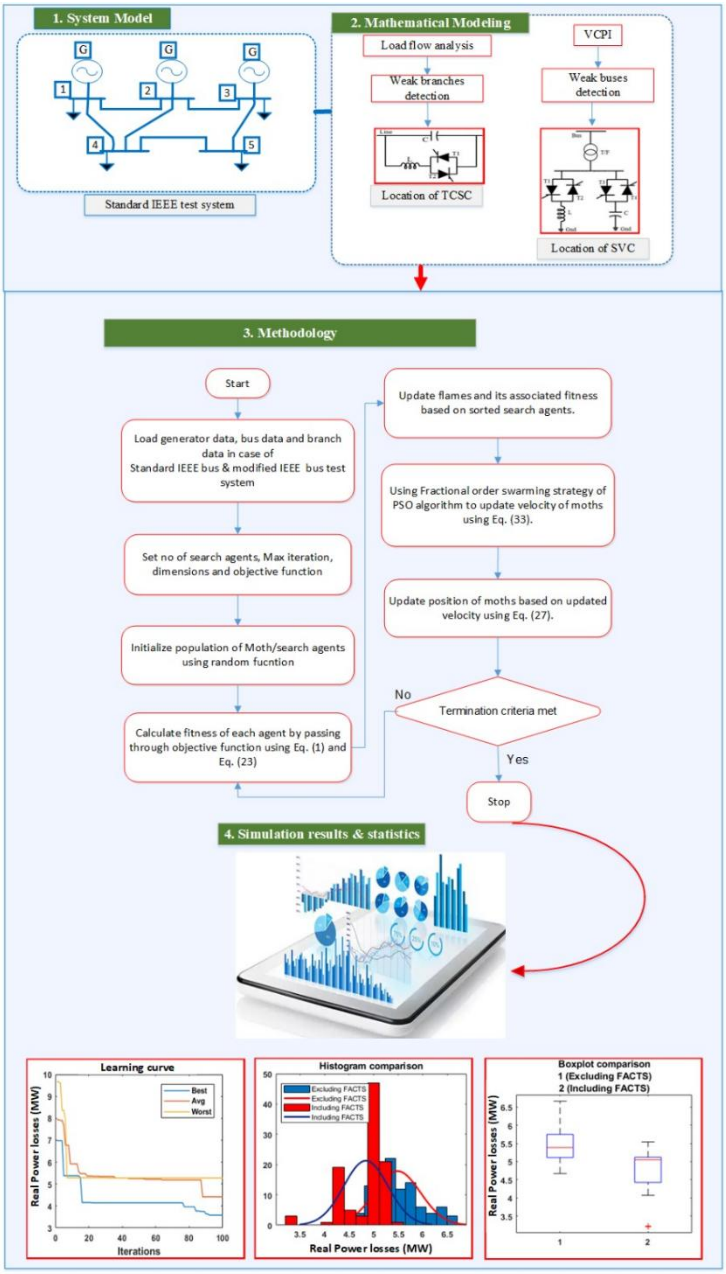

Figure 4. Graphical abstract of proposed FMFO algorithm for solving ORPD problem.

4. Discussion

It is a common practice to evaluate the performance of newly developed algorithms on a set of well-known benchmark functions with known global optima. The same methodology is applied in this case, using benchmark functions for comparison purposes from [63–66].

Benchmark functions are categorized into two distinct groups, namely unimodal and multimodal. Since unimodal functions only have one global optimum with no local optima, the exploitation of algorithms is suitable to be benchmarked for such functions. In contrast, multimodal functions have many local optima and are useful to study the exploration and avoidance of local optima by algorithms. The fractional Grünwald-Letnikov operator provides power-law memory kernels whose decay rate depends on the fractional order q. Lower q leads to larger memory and enhanced exploration. In contrast, greater values of q have the effect of diminishing memory impacts and increasing the rate of convergence, leading to improved exploitation. To justify the theoretical hypothesis put forward, further experiments were done using benchmark unimodal and multimodal functions. Unimodal functions assess mostly the ability to exploit, since there is only one global optimum present, while multimodal functions assess the ability to explore, since there are multiple local optima present.

Accordingly, the appropriate fractional order cannot be seen as a problem-dependent tuning parameter. It is determined by the characteristics of the landscape of the optimization problem. The problems that have very multimodal search spaces will prefer small values of the fractional order, since exploration will be improved, while smooth and unimodal search spaces will prefer high orders for good exploitation.

The benchmark functions in unimodal ($b1$–$b4$) and multimodal ($b5$–$b8$) categories are formulated mathematically in Table 1. The original unimodal and multimodal benchmark functions are not complex enough; therefore, they were altered to increase their complexity.

Table 1. Mathematical representation of unimodal ($b1$–$b4$) and multimodal ($b5$–$b8$) benchmark functions.

Benchmark functions
$b1(y) = \sum_{i=1}^{n} y_i^2$
$b2(y) = \sum_{i=1}^{n} \lvert y_i \rvert + \prod_{i-1}^{n} \lvert y_i \rvert$
$b3(y) = \sum_{i-1}^{n-1} \left[100\left(y_{i+1} - y_i^2\right)^2 + (y_i - 1)^2\right]$
$b4(y) = \sum_{i-1}^{n} (\lfloor y_i + 0.5 \rfloor)^2$
$b5(y) = \sum_{i-1}^{n} [y_i^2 - 10\cos(2\pi y_i) + 10]$
$b6(y) = -20\exp\left(-0.2\sqrt{\frac{1}{n}\sum_{i=1}^{n} y_i^2}\right) - \exp\left(\frac{1}{n}\sum_{i=1}^{n}\cos(2\pi y_i)\right) + 20 + e$
$b7(y) = \frac{1}{4000}\sum_{i=1}^{n} y_i^2 - \prod_{i=1}^{n}\cos\left(\frac{y_i}{\sqrt{i}}\right) + 1$
$b8(y) = 0.1\left[\sin^2(3\pi y_1) + \sum_{k=1}^{s}(y_k - 1)^2\left(1 + \sin^2(3\pi y_{k+1})\right) + (y_s - 1)^2\left(1 + \sin^2(2\pi y_m)\right)\right] + \sum_{k=1}^{m} u(y_k, 10,100,4)$

Simulations were performed against benchmark functions ($b1$–$b8$) under a range of fractional orders from 0.1 to 0.9. To ensure statistical reliability, 30 independent runs are conducted, and the minimum of the best-obtained values is reported as the representative outcome. These evaluations are performed across a range of queue fractions $\alpha \in [0.1, ..., 0.9]$ for all unimodal and multimodal test functions. Table 2 presents the best fitness values achieved for both unimodal and multimodal benchmark functions, across the full range of α values based on 30 independent trials. These results demonstrate that FMFO acquires minimal objective function values, which justifies the superiority of the logarithmic spiral between exploration and exploitation. The objective function values of each combination give clarify the effects of fractional calculus on the search dynamics, trade-off between exploration and exploitation, and convergence stability. The lower fractional orders $\alpha \in [0.1, ..., 0.5]$ have smaller objective function values for multimodal benchmark functions, which indicate a faster approach to convergence and the high strength of exploration. With higher fractional orders α approaching 1.0, performance is likely to decrease, indicating that there is too much momentum or instability in the process of searching.

Table 2. Performance comparison of FMFO across different fractional α from 0.1 to 0.9.

Functions	0.1	0.2	0.3	0.4	0.5	0.6	0.7	0.8	0.9
b1	0.137	0.122	0.095	0.087	0.041	0.090	0.068	0.065	0.025
b2	0.483	0.449	0.515	0.432	0.288	0.361	0.227	0.296	0.187
b3	0.008	0.008	0.008	0.006	0.005	0.004	0.003	0.005	0.003
b4	0.021	0.026	0.027	0.017	0.016	0.016	0.018	0.014	0.009
b5	0.626	1.013	1.103	1.110	1.371	1.605	1.372	1.287	1.487
b6	31.673	40.021	42.136	36.352	41.015	48.518	48.004	46.046	70.269
b7	0.043	0.046	0.054	0.072	0.110	0.070	0.090	0.106	0.149
b8	60.993	77.795	76.926	97.536	97.264	105.184	120.943	113.656	110.674

The assessment of the FMFO was executed by comparing the mean fitness values with state-of-the-art algorithms from the literature, such as GA [67], FA [68], SMS [69], FPA [70], BA [71], GSA [72], and PSO [73], as listed in Table 3. It is important to note that each algorithm is executed using a population of 30 search agents over 1000 iterations. This empirical choice of 30 search agents strikes a balance between computational efficiency and the likelihood of reaching a global optimum. Increasing the number of search agents generally enhances the probability of locating the global minimum; however, 30 has been deemed a reasonable compromise given the computational demands of optimization problems. As shown in Table 3, the FMFO method delivers results that are highly competitive with other algorithms across both unimodal and multimodal benchmark functions. Unimodal functions are particularly useful for assessing an algorithm's exploitation capability, while multimodal functions evaluate exploration performance. The results, therefore, highlight that FMFO exhibits strong abilities in both exploitation and exploration.

Table 3. Comparison of FMFO optimal results on unimodal and multimodal benchmark functions with literature.

Algorithms	b1	b2	b3	b4	b5	b6	b7	b8
BA	20792.44	89.78561	1995125	17053.41	96.21527	15.94609	220.2812	$1.09E+08$
GSA	608.2328	22.75268	741.003	3080.964	31.00014	3.740988	0.486826	7.617114
SMS	120	0.020531	6382246	41439.39	152.8442	19.13259	420.5251	1E+08
PSO	1.321152	7.715564	77360.83	286.6518	124.2973	9.167938	12.41865	11813.5
FA	7480.746	39.32533	3795009	7828.726	214.8951	14.56769	69.65755	5557661
FPA	203.6389	11.1687	10974.95	175.3808	92.69172	6.844839	2.716079	62.3985
GA	21886.03	56.51757	31321418	20964.83	236.8264	17.84619	179.9046	$1.08E+08$
MFO	0.1233	0.7466	0.0067	0.0484	1.5224	119.105	0.1820	113.892
FMFO	0.09156	2.31149	160.84771	0.09482	110.57847	0.87358	0.12357	0.028403

Furthermore, a nonparametric Wilcoxon rank-sum test was used to statistically justify the performance of the proposed FMFO algorithm over the simple MFO on eight benchmark functions ($b1$–$b8$). This test has been chosen as it is strong enough to compare two independent samples. The statistical measures of Table 4 indicate that the mean and median fitness values produced by FMFO are significantly and consistently lower than the basic MFO, indicating a better convergence accuracy and optimization efficiency. Moreover, the standard deviations of FMFO are much lower, which means that it has increased stability and lesser variance in multiple runs. All test functions have negative values of the Z-statistic, which proves that FMFO has shown more (lower) fitness results than MFO. Above all, all p-values are very low (below the significance level 0.05), with values of 1.23×10^{-5} to $6.15 \times 10^{-6,}$ and this is solid statistical evidence to reject the null hypothesis. These findings affirm that the gains are not caused by chance but are those resulting on actual improvement in the performance of the algorithms. As a result, the proposed FMFO is significantly more precise in convergence, quality of the solution, and overall robustness compared to the canonical MFO, in terms of performance in various optimization landscapes.

Furthermore, the efficacy and application of the FMFO algorithm for ORPD planning, including four test cases, have been examined. The FMFO algorithm was applied with variation of fractional orders from 0.1 to 0.9 with an increment of 0.1 in each step, i.e., FMFO-1 to FMFO-9. In our first test case, we utilized the widely recognized standard IEEE 30 bus test system as the basis for our analysis in reducing real power losses. In our second test case, we extended the standard 30 IEEE bus test system as a modified 30 IEEE bus test case by introducing FACTS devices. The addition of FACTS devices has shown to be a significant advancement, improving power flow and further reducing real power losses. In the third test case, the standard IEEE 57 bus test system was adopted to reduce voltage deviations. Finally, we extended our investigation to a modified IEEE 57 bus test case by adding FACTS devices to reduce real power losses explicitly. Table 5 tabulates the parameters settings of the FMFO algorithm across all test cases.

Table 4. Wilcoxon rank-sum test results between MFO and FMFO across benchmark functions.

Test	Algorithm	Mean	Median	Std. Deviation	Statistic (Z)	p-value	Significance
b_1	MFO	2666.6672	0.0002	5832.9226	-	-	-
	FMFO	0.0916	0.0959	0.0319	-4.37	1.23×10^{-5}	Significant
b_2	MFO	32.0022	30.0001	22.0332	-	-	-
	FMFO	2.3115	1.3278	3.0508	-4.68	2.83×10^{-6}	Significant
b_3	MFO	9669.7904	344.4678	27264.0659	-	-	-
	FMFO	160.8477	124.3152	135.1463	-4.52	6.15×10^{-6}	Significant
b_4	MFO	1683.3751	0.0001	3828.4898	-	-	-
	FMFO	0.0948	0.0897	0.0435	-3.45	0.0006	Significant
b_5	MFO	157.1814	151.9083	49.3557	-	-	-
	FMFO	110.5785	104.4415	37.0855	-3.99	6.6×10^{-5}	Significant
b_6	MFO	14.2054	19.1459	7.9130	-	-	-
	FMFO	0.8736	0.3864	2.6547	-4.58	4.6×10^{-6}	Significant
b_7	MFO	12.0688	0.0186	31.2357	-	-	-
	FMFO	0.1236	0.0511	0.3097	-3.91	9.2×10^{-5}	Significant
b_8	MFO	0.4036	0.1129	0.6621	-	-	-
	FMFO	0.0284	0.0262	0.0112	-4.19	2.8×10^{-5}	Significant

Table 5. Parameters settings of FMFO.

Test cases	Moth's dimensions	Population size	Best fractional - order derivatives	Cognitive/social constants	Maximum iterations	Independent trials
Case A	13	20	0.9	0.9/1.5	100	100
Case B	17	20	0.5	0.9/1.5	100	100
Case C	25	20	0.3	0.9/15	500	20
Case D	25	20	0.3	0.9/15	500	20

Algorithm 1. FMFO

INPUT: Test data for standard IEEE and modified IEEE test systems are loaded.
OUTPUT: The optimal outcomes for real power losses and voltage deviations are achieved by fitness evaluation of the objective functions.
Initialization. Random initialize the moths through the inclusion of n agents, with dimensions according to the controlled variables.
Evaluating fitness. Each search agent's fitness is assessed by applying the necessary objective functions for real power losses and voltage deviations, which are described in Eqs (2.1) and (2.15), respectively.
Sorting based on fitness. Distribute the search agents from the initial population into the flame population by sorting them according to their fitness function values.
Position update mechanism. For updating the position of a moth that corresponds to the best flame, a logarithmic spiral function is used as described in Eq (3.2).
Velocity update mechanism. Fractional orders between 0.1 and 0.9 are employed to ascertain the velocity for each ith moth as described in Eq (3.18).
Termination criteria. The termination criteria are predicated on a specified iteration. When the total number of iterations achieve a specified limit, the algorithm will end its operation. If the stopping criteria have not been satisfied, go to the "Fitness Evaluation" stage with a modified population of moths; otherwise, proceed.
Results storage. The global best particle parameters are stored according to the least values of real power losses and voltage deviations.
Statistical analysis. One hundred independent runs are subjected to statistical analysis using histograms, boxplots, and cumulative distribution function assessments.

4.1. Case A: IEEE 30 bus test case to minimize real power losses

Case A applies to the IEEE 30 bus system to evaluate the FMFO algorithm's effectiveness in minimizing real power losses. Configuration of IEEE 30 bus for case A is given in Table 6. Operating limits of variables for case A are given in Table 7. Outcomes of controlled variables utilizing several algorithms from the literature for test case A are given in Table 8. Against a base power loss of 5.663 MW, FMFO achieves a 17.53% reduction, outperforming HSA, IWO, DE, GA, and ICA. Compared to the base case value of 5.663 MW, the performance of the MFO technique led to a decrease of 16.93%, resulting in an objective value of 4.7043 MW. The proposed FMFO method decreased the objective value to 4.6701 MW, corresponding to a 17.53% reduction. This suggests that fractional-order dynamics inclusion improves the performance of the optimization algorithm, leading to better reduction by FMFO compared to the MFO method. Figure 5 shows convergence trends for fractional orders from 0.1 to 0.9 over 100 iterations and trials. At q=0.1, losses are 4.7479 MW, improving to 4.6726 MW at q=0.2. Losses vary slightly across q=0.3 to 0.8, with the best result being 4.6701 MW at q=0.9. Voltage profiles for case A are displayed in Figure 6.

Table 6. Configuration of IEEE 30 bus for case A.

Index.	Components	Quantity	Configuration of components
1	Power generating units	6	At buses 1, 2, 5, 8, 11 and 13
2	Transformers	4	Located at branches 4-12, 6-10, 6-9 and 27-28
3	Branches	41	-
4	Capacitors	3	Located at buses 3, 10 and 24

Table 7. Operating limits of variables for case A.

Index.	Variables	Lower limit	Upper limit
1	Generator bus voltages	0.9	1.1
2	Load bus voltages	0.9	1.1
3	Transformer's tap position settings	0.9	1
4	Static shunt capacitors	-30	30

Table 8. Outcomes of controlled variables utilizing several algorithms from literature for test case A.

Controlled variables	Reported results							Proposed	
	DE [34]	GA [74]	PSO [35]	HSA [36]	ICA [37]	MICA-IWO [37]	IWO [38]	MFO	FMFO
V_{G1}	1.09532	1.0721	1.0313	1.0726	1.0785	1.0797	1.06965	1.1000	1.1000
V_{G2}	1.08595	1.063	1.0114	1.0625	1.06943	1.0705	1.06038	1.0908	1.0932
V_{G5}	1.06263	1.0377	1.0221	1.0399	1.06943	1.0483	1.03692	1.0733	1.0714
V_{G8}	1.06508	1.0445	1.0031	1.0422	1.04714	1.0486	1.03864	1.0651	1.0737
V_{G11}	1.0266	1.0132	0.9744	1.0318	1.03485	1.0751	1.02973	1.1000	1.0905
V_{G13}	1.01425	1.0898	0.9987	1.0681	1.07106	1.0707	1.05574	1.0758	1.1000
T_1	1.0178	1.0221	0.97	1.01	1.08	1.03	1.05	1.0500	0.9726
T_2	0.97928	0.9917	1.02	1	0.95	0.99	0.96	0.9000	0.9217
T_3	0.97784	0.9964	1.01	0.99	1	1	0.97	0.9476	0.9746
T_4	1.00894	0.971	0.99	0.97	0.97	0.98	0.97	0.9554	0.9534
$Q_{VAR\,3}$	20.2236	5.3502	17	34	-6	-7	8	17.0895	3.3864
Q_{VAR10}	9.58433	36	13	12	36	23	35	16.7964	8.7710
Q_{VAR24}	13.0299	12.4175	23	10	11	12	11	10.3902	8.5701
P_{LOSS} (MW)	4.888	4.877	5.881	5.109	4.849	4.846	4.92	4.7043	4.6701

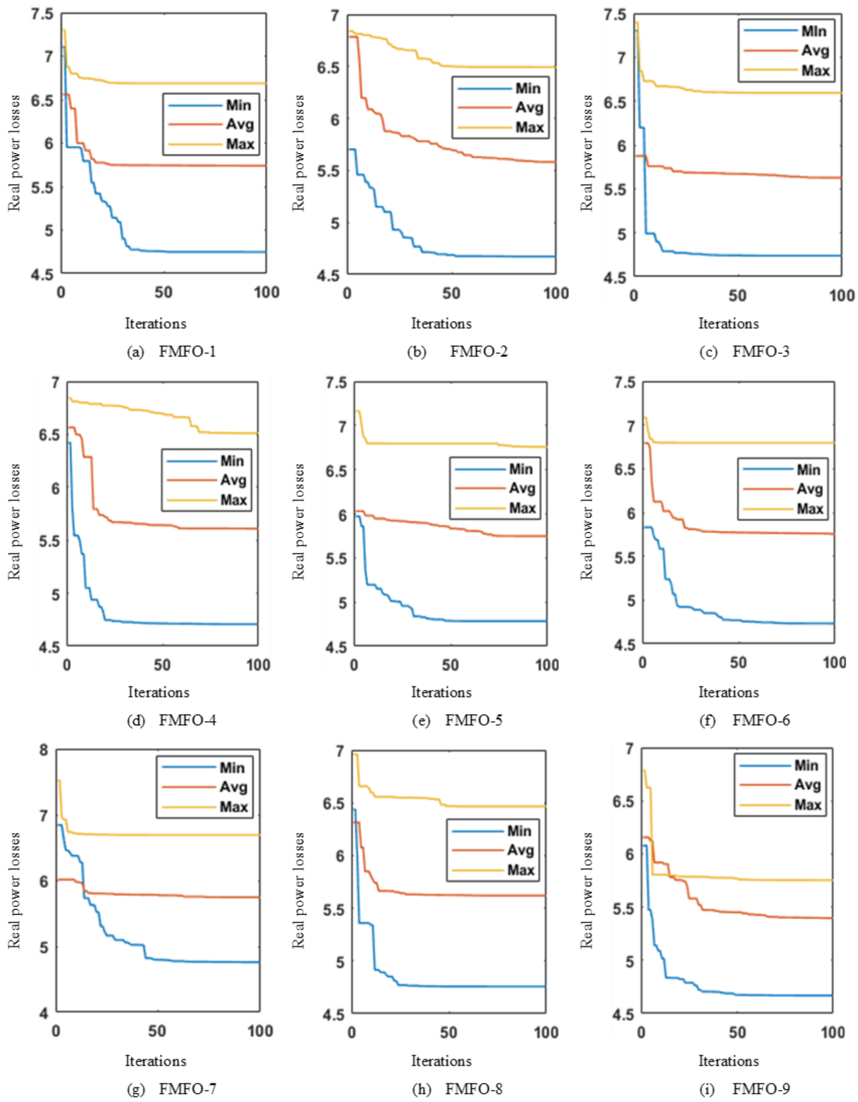

Figure 5. FMFO convergence curve of real power losses for case A at different fractional orders.

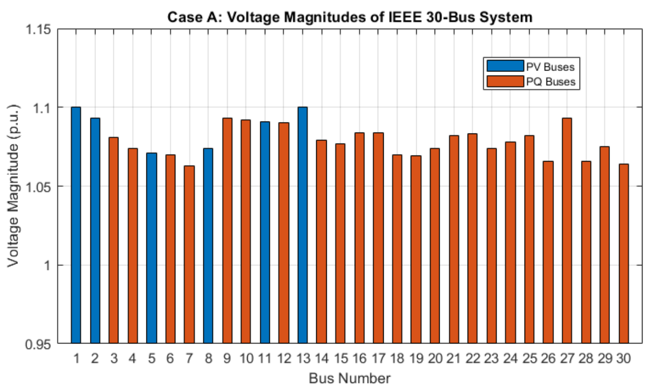

Figure 6. Voltage magnitudes of buses including PV and PQ buses for test case A.

4.2. Case B: Modified IEEE 30 bus test case to minimize real power losses

The IEEE 30 bus system, including FACTS devices, is implemented as the second test case. The results of the research referenced in [26] have been incorporated into our current study. Configuration of the modified IEEE 30 bus test system for case B is given in Table 9. Operating limits of variables for test case B are tabulated in Table 10.

Table 9. Configuration of modified IEEE 30 bus test system for case B.

Index	Components	Quantity	Configuration of components
1	Power generating units	6	At buses 1, 2, 5, 8, 11 and 13
2	Transformers	4	Located at branches 4-12, 6-10, 6-9 and 27-28
3	Branches	41	-
4	TCSC	4	Located at branches 5, 25, 28 and 41
5	SVC	4	At buses 4, 20, 22 and 28

Table 10. Operating limits of variables for case B.

Index	Variables	Lower limit	Upper limit
1	Generator bus voltages	0.9	1.1
2	Load bus voltages	0.9	1.1
3	Transformer's tap position settings	0.9	1
4	TCSC	0	0.08
5	SVC	0	0.20

The load flow study identified branches 5, 25, 28, and 41 as the most vulnerable and recommended the installation of TCSCs to mitigate the risk. This conclusion was drawn based on their respective initial reactive power losses of 3.83 Mvar, 0.16 Mvar, 0.14 Mvar, and 0.13 Mvar, as shown in Table 11.

Table 11. Active and reactive power flows based on the load flow method to determine weak branches for case B.

Branch	From bus	To bus	From bus		To bus		Losses	
			Active power (MW)	Reactive power (MVAR)	Active power (MW)	Reactive power (MVAR)	Active power (MW)	Reactive power (MVAR)
5	2	5	45.20	4.51	-44.29	-5.07	0.912	3.83
25	10	20	8.37	0.73	-8.30	-0.57	0.072	0.16
28	10	22	7.97	4.65	-7.90	-4.51	0.068	0.14
41	6	28	14.29	3.71	-14.25	-4.92	0.037	0.13

After the implementation of TCSC devices, a notable decrease in losses was seen. This led to reactive power losses of 2.81 Mvar for branch 5, 0.14 Mvar for branch 25, 0.12 Mvar for branch 28, and 0.07 Mvar for branch 41, as shown in Table 12. In addition, the buses 4, 20, 22, and 28 are vulnerable ones, making them perfect for SVC device placement using the VCPI technique described in [26]. Subsequently, after the installation of SVC devices, we saw a significant rise in the voltage magnitudes of these buses, as shown in Table 13. Bus voltage magnitudes for case B are illustrated in Figure 7.

Table 12. Active and reactive power flows due to load flows after installing TCSC for case B.

Branch	From bus	To bus	From bus		To bus		Losses	
			Active power (MW)	Reactive power (MVAR)	Active power (MW)	Reactive power (MVAR)	Active power (MW)	Reactive power (MVAR)
5	2	5	39.69	-12.25	-39.02	10.12	0.669	2.81
25	10	20	7.93	1.49	-7.87	-1.36	0.061	0.14
28	10	22	7.92	4.32	-7.86	-4.19	0.060	0.12
41	6	28	11.72	1.25	-11.70	-2.70	0.020	0.07

Table 13. VCPI based on weak bus voltages magnitude before and after installing SVC for case B.

Bus #	Before FACTS	After FACTS
4	1.022	1.083
20	0.945	0.986
22	0.941	0.984
28	1.012	1.081

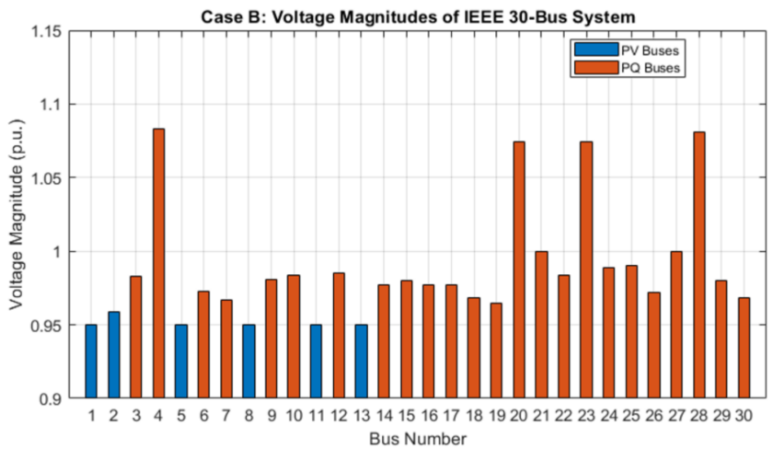

Figure 7. Voltage magnitudes of buses including PV and PQ buses for test case B.

The FMFO algorithm, using 20 particles, was applied to minimize real power losses. Figure 8 shows convergence trends for fractional orders from 0.1 to 0.9 over 100 iterations and trials. Losses decreased from 4.0776 MW at q=0.1 to a minimum of 3.210 MW at q=0.5, which also recorded an average of 4.3873 MW and a maximum of 5.5374 MW. Other notable results include 3.7819 MW at q=0.2, 3.2221 MW at q=0.9, and slightly higher values at q=0.7 and 0.8.

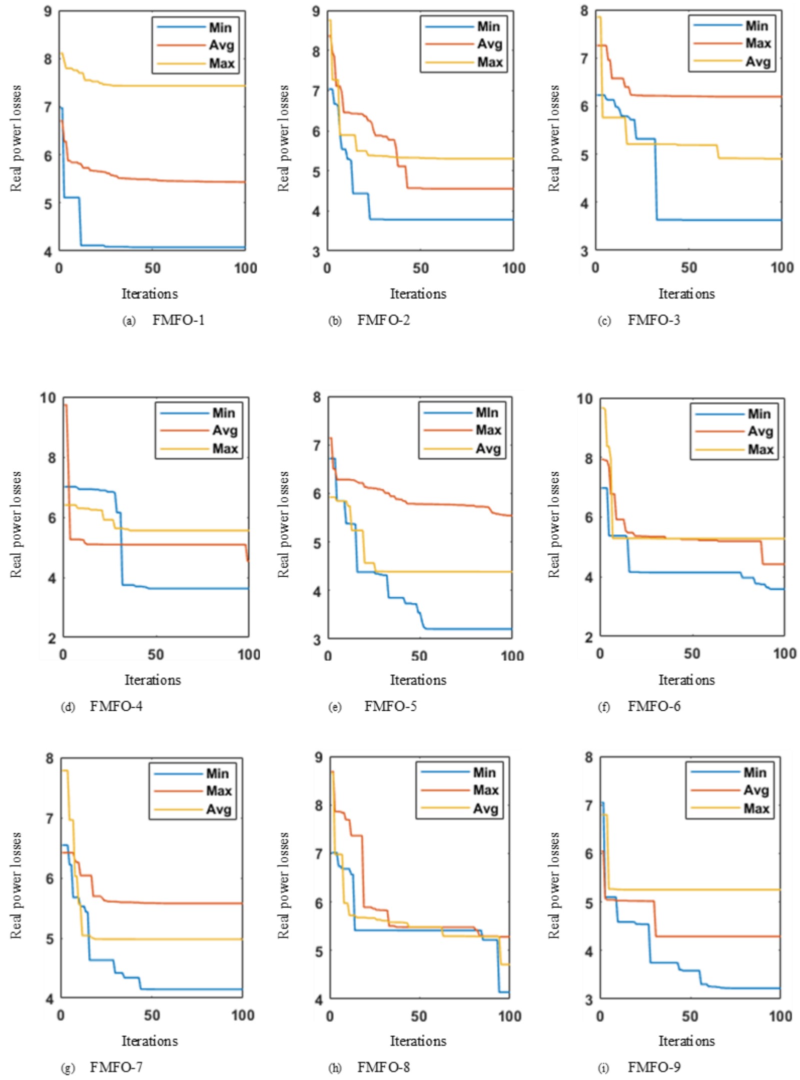

Figure 8. FMFO convergence curve of real power losses for case B at different fractional orders.

Table 14 compares FMFO's control outputs with other methods, showing the highest loss reduction of 43.32% versus 5.663 MW baseline, outperforming Fuzzy-DE (16.21%), DE (13.81%), QODE (6.76%), GWO (12.96%), EPSO (10.84%), APSO (10.08%), and FODPSO (17.30%). Compared to the base case value of 5.663 MW, the performance of the MFO technique led to a decrease of 27.04%, resulting in an objective value of 4.132 MW. The proposed FMFO method decreased the objective value to 3.210 MW, corresponding to a 43.32% reduction. This suggests that fractional- order dynamics inclusion improves the performance of the optimization algorithm, leading to better reduction by FMFO compared to MFO method.

Table 14. Outcomes of controlled variables utilizing several algorithms from literature for test case B.

	Reported results							Proposed	
Controlled variables	Fuzzy-DE [75]	DE [75]	QODE [76]	GWO [76]	EPSO [29]	APSO [29]	FO-DPSO [29]	MFO	FMFO
Q_{G2}	0.000	-0.509	0.354	-0.011	0.600	0.000	0.749	0.105	-0.145
Q_{G5}	0.600	-0.131	0.237	-0.115	0.000	0.000	0.439	0.400	-0.006
Q_{G8}	0.250	0.396	0.446	0.123	0.000	0.000	0.388	-0.082	0.052
Q_{G11}	0.041	0.303	0.350	0.080	0.400	0.400	0.266	-0.047	0.016
Q_{G13}	0.000	0.047	0.246	0.212	0.000	0.000	0.847	-0.007	0.100
T_1	0.978	0.902	0.901	0.900	0.944	0.900	0.989	0.900	0.900
T_2	0.900	0.966	0.951	0.930	0.900	0.950	1.007	0.900	0.900
T_3	0.937	0.901	0.900	0.900	0.900	0.918	0.997	0.900	0.900
T_4	0.915	0.921	0.928	0.929	0.933	0.933	0.979	0.900	0.900
$TCSC_1$	0.000	0.080	0.062	0.080	0.146	0.146	0.111	0.000	0.000
$TCSC_2$	0.000	0.080	0.159	0.080	0.042	0.042	0.273	0.047	0.031
$TCSC_3$	0.000	0.080	0.200	0.080	0.105	0.105	0.090	0.006	0.020
$TCSC_4$	0.000	0.080	0.012	0.080	0.137	0.139	0.135	0.000	0.007
SVC_1	0.000	0.066	0.080	0.037	0.000	0.000	0.200	0.093	0.056
SVC_2	0.000	0.149	0.080	0.171	0.000	0.000	0.200	0.000	0.179
SVC_3	0.000	0.150	0.079	0.200	0.000	0.000	0.200	0.017	0.013
SVC_4	-	0.023	0.080	0.005	0.000	0.077	0.200	0.069	0.086
P_{Loss} (MW)	4.745	4.881	5.28	4.929	5.049	5.092	4.683	4.132	3.210

4.3. Case C: IEEE 57 bus test case to curtail voltage deviation

Case C applies the IEEE 57-bus system to evaluate the FMFO algorithm's effectiveness in minimizing voltage deviation. FMFO outputs across fractional orders (α = 0.1 to 0.9) are provided in Table 15. Operating limits of variables for case C are tabulated in Table 16. Table 17 compares FMFO's minimal voltage deviation with other optimization techniques from the literature, including PSO, CLPSO, fractional PSO gravitational search algorithm (FPSOGSA), FPSOGSA-E, fractional order Darwinian PSO (FODPSO), ICA-PSO, SGA, WOA, EO, LAPO, MPA, SCA, and ALO. Table 18 presents their respective control variable outputs. Compared to the base case voltage deviation of 4.1788 p. u, FMFO achieved the highest reduction of 84%. Figure 9 shows convergence behavior over 500 iterations across fractional orders. Fastest convergence and low variability were observed at q=0.1, 0.5 and 0.3. q=0.9 and 0.8 showed steady but more varied trends, while q=0.6 had moderate trends. Bus voltage magnitudes for case C are illustrated in Figure 10.

Table 15. Comparison of proposed FMFO algorithm in terms of fractional orders (q=0.1 to 0.9) for test case C**.**

Variables	FMFO-1	FMFO-2	FMFO-3	FMFO-4	FMFO-5	FMFO-6	FMFO-7	FMFO-8	FMFO-9
V_{G1}	1.0193	1.0195	1.0154	1.0285	1.0199	1.0189	1.0185	1.0423	1.0184
V_{G2}	0.9892	0.9590	1.0108	0.9660	0.9587	0.9627	1.0982	1.0775	1.0226
V_{G3}	1.0261	1.0156	1.0189	1.0104	1.0158	1.0157	1.0096	1.0043	1.0150
V_{G6}	0.9987	0.9802	1.0014	1.0012	1.0019	1.0021	1.0034	1.0055	1.0013
V_{G8}	1.0261	1.0397	1.0241	1.0266	1.0235	1.0195	1.0259	1.0217	1.0464
V_{G9}	1.0278	1.0358	1.0256	1.0471	1.0409	1.0260	1.0539	1.0797	1.0474
V_{G12}	1.0037	1.0045	1.0104	1.0010	1.0046	1.0051	1.0050	0.9638	1.0051
T_1	1.0486	1.0711	0.9201	0.9855	0.9000	1.0592	0.9872	1.0556	1.0429
T_2	0.9556	0.9152	1.0453	0.9781	1.0717	0.9181	0.9888	0.9188	0.9411
T_3	0.9708	0.9745	0.9736	0.9779	0.9756	0.9782	0.9732	0.9759	0.9776
T_4	1.0570	1.0587	1.0513	1.0681	1.0501	1.0590	1.0732	1.0569	1.0557
T_5	0.9504	0.9486	0.9516	0.9461	0.9526	0.9472	0.9446	0.9502	0.9593
T_6	0.9055	0.9092	0.9060	0.9065	0.9051	0.9062	0.9087	0.9080	0.9100
T_7	0.9000	0.9000	0.9001	0.9000	0.9000	0.9045	0.9000	0.9000	0.9000
T_8	0.9333	0.9242	0.9219	0.9023	0.9152	0.9335	1.0058	0.9321	0.9054
T_9	0.9837	0.9950	0.9916	1.0032	0.9858	0.9772	0.9202	0.9876	0.9939
T_{10}	1.0051	1.0031	1.0080	1.0005	1.0122	0.9855	1.0183	0.9904	1.0132
T_{11}	0.9000	0.9000	0.9000	0.9000	0.9000	0.9118	0.9000	0.9061	0.9096
T_{12}	0.9616	0.9388	0.9417	0.9955	0.9835	0.9458	1.0115	0.9665	0.9607
T_{13}	1.0310	1.0796	1.0554	1.0273	1.0048	1.0470	1.0204	1.0761	1.0870
T_{14}	0.9172	0.9214	0.9174	0.9025	0.9094	0.9034	0.9046	0.9344	0.9000
T_{15}	0.9950	1.0055	0.9903	1.0118	1.0016	0.9935	1.0249	1.0423	1.0100
Q_{VAR18}	1.4645	0.1850	0.5650	0.4757	2.3729	0.1481	2.9870	1.4036	0.0009
Q_{VAR25}	4.6997	4.3676	4.8257	3.6203	4.8379	4.9322	4.9788	4.6107	3.9482
Q_{VAR53}	4.9581	4.3963	3.6149	2.9339	2.3591	4.9340	3.6415	3.7034	1.9676
V.D (p.u)	0.6710	0.6829	0.6687	0.6854	0.6710	0.6744	0.6959	0.7024	0.7037

Table 16. Operating limits of variables for case C.

Index	Variables	Lower limit	Upper limit
1	Generator bus voltages	0.95	1.1
2	Load bus voltages	0.95	1.1
3	Transformer's tap position settings	0.9	1.1
4	Static shunt capacitors	-30	30

Table 17. Comparative analysis of voltage deviations from the literature for test case C.

Algorithm	V.D	Algorithm	V.D	Algorithm	V.D
PSO [78]	0.8007	ICA-PSO [78]	0.7130	ICA [78]	0.7952
CLPSO [79]	1.0929	SGA [80]	2.7021	MPA [82]	0.6927
FPSOGSA [74]	0.8017	WOA [76]	0.7176	SCA [82]	1.1187
FPSOGSA-E [77]	0.7378	EO [82]	0.7778	ALO [82]	0.7560
FODPSO [29]	0.7102	LAPO [81]	0.6893	FMFO	0.6687

Table 18. Outcomes of controlled variables utilizing several algorithms from the literature for test case C.

Controlled variables	Base case	FPSO-GSA	FO-DPSO	LAPO	MPA	SCA	ALO	WOA	EO	FMFO
V_{G1}	1.0400	1.1000	1.04	1.0350	1.0057	0.9568	1.0325	1.0470	0.9966	1.0154
V_{G2}	1.0100	1.0987	1.0298	1.0472	0.9858	0.9087	1.0253	1.0792	1.0018	1.0108
V_{G3}	0.9850	1.0871	1.0099	1.0470	1.0414	1.0247	1.0305	1.0474	1.0054	1.0189
V_{G6}	0.9800	1.0807	0.9776	0.9974	1.0002	1.0245	1.0105	1.0208	1.0085	1.0014
V_{G8}	1.0500	1.1000	0.9855	0.9926	0.9978	1.0366	0.9984	0.9992	1.0447	1.0241
V_{G9}	0.9800	1.0845	0.9676	0.9978	1.0239	0.9785	0.9467	1.0188	1.0137	1.0256
V_{G12}	1.0150	0.9600	0.9081	1.0479	1.0155	1.0539	1.0192	0.9896	1.0389	1.0104
T_1	0.9700	1.0071	4	0.9834	0.9793	0.9516	0.9342	0.9316	0.9710	0.9201
T_2	0.9780	1.0847	15	0.9934	0.9753	0.9943	1.0241	1.0270	0.9919	1.0453
T_3	1.0430	0.9959	11.678	1.0008	0.9847	1.0546	0.9892	0.9934	0.9810	0.9736
T_4	1.0430	0.9908	0.9	1.0076	1.0090	1.0308	0.9975	0.9829	1.0809	1.0513
T_5	0.9670	0.9964	0.9209	0.9792	1.0084	0.9807	1.0071	1.0128	1.0109	0.9516
T_6	0.9650	0.0072	1.0268	0.9764	1.0072	1.0097	0.9794	0.9393	0.9593	0.9060
T_7	0.9550	0.9900	1.0075	0.9621	0.9497	1.0373	1.0105	0.9493	1.0178	0.9001
T_8	0.9550	0.9906	0.9070	0.9781	1.0113	0.9328	0.9770	1.0021	1.0198	0.9219
T_9	0.9000	1.0028	0.9871	1.0095	0.9363	0.9456	0.9876	0.9878	1.0011	0.9916
T_{10}	0.9300	0.9900	0.9010	0.9907	1.0126	0.9451	0.9992	0.9078	1.0188	1.0080
T_{11}	0.8950	1.0027	0.9	0.9293	0.9395	0.9816	0.9445	0.9265	0.9158	0.9000
T_{12}	0.9580	1.0844	0.9	0.9619	0.9860	0.9352	0.9933	0.9357	0.9519	0.9417
T_{13}	0.9580	1.0023	0.9165	0.9558	0.9023	1.0026	0.9535	0.9103	0.9631	1.0554
T_{14}	0.9800	0.9900	0.9	0.9607	0.9624	1.0020	0.9764	0.9651	0.9282	0.9174
T_{15}	0.9400	1.0951	0.9	0.9891	0.9925	0.9958	0.9553	1.0114	1.0226	0.9903
Q_{VAR18}	0.0000	4.9846	0.9980	3.3741	4.5500	2.9945	4.4408	4.4842	4.5238	0.5650
Q_{VAR25}	0.0000	4.9992	0.9945	2.0325	2.4172	2.1072	2.1933	1.4313	1.7584	4.8257
Q_{VAR53}	0.0000	4.3653	0.9	3.1252	4.4643	2.6531	3.5383	4.1241	2.3706	3.6149

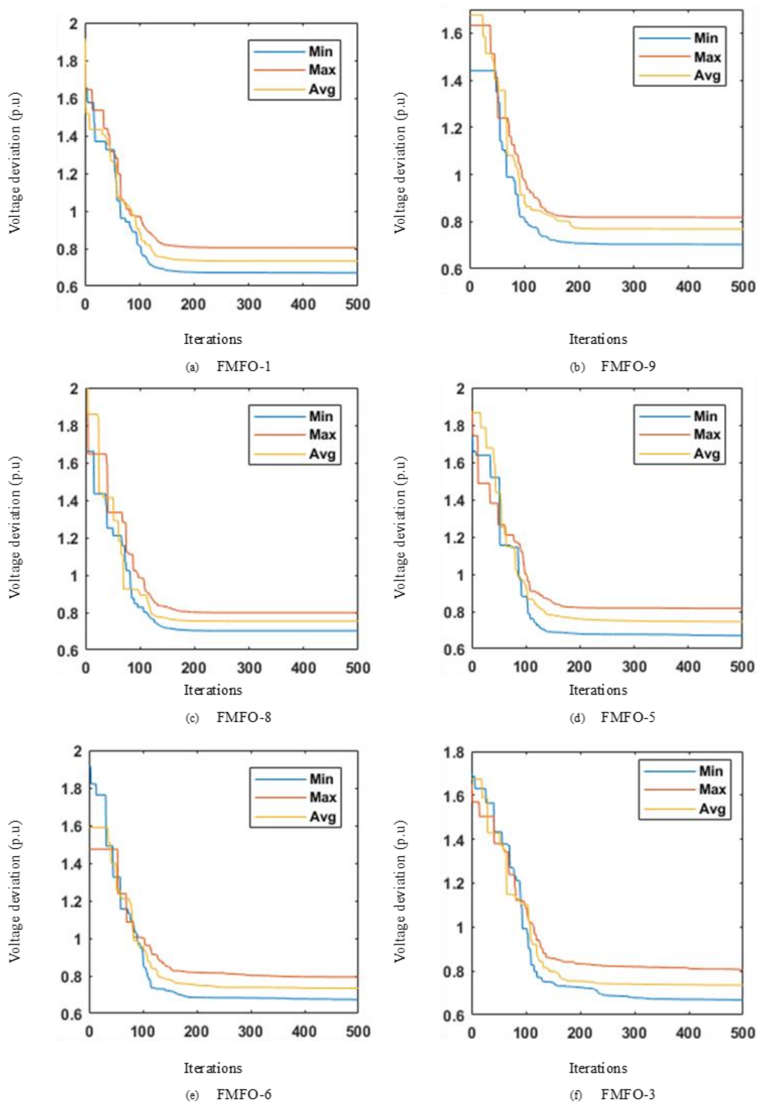

Figure 9. FMFO convergence curve of voltage deviations for case C at different fractional orders.

4.4. Case D: Modified 57 IEEE bus test case to curtail real power losses

The fourth case corresponds to the implementation of the modified IEEE 57 bus system. Configuration of modified IEEE 57 bus test system for case D is given in Table 19. The parameter settings for the proposed FMFO in test case D are listed in Table 20. The load flow identified branches 13, 37, 57, and 61 as the most susceptible and suggested the implementation of TCSCs to reduce the risk. The conclusion was made by considering the initial reactive power losses of 0.29 Mvar, 0.06 Mvar, 0.35 Mvar, and 0.10 Mvar for each respective branch, as presented in Table 21. Following the deployment of TCSC devices, a significant reduction in losses was observed. Table 22 shows that branch 13 had reactive power losses of 0.19 Mvar, branch 37 had losses of 0.04 Mvar, branch 57 had losses of 0.13 Mvar, and branch 61 had losses of 0.07 Mvar. Furthermore, it was discovered that buses 4, 20, 22, and 28 are susceptible to attacks, making them ideal candidates for the implantation of SVC devices utilizing the VCPI technique outlined in [6]. Following the installation of SVC devices, we observed a substantial increase in the voltage magnitudes of these buses, as indicated in Table 23.

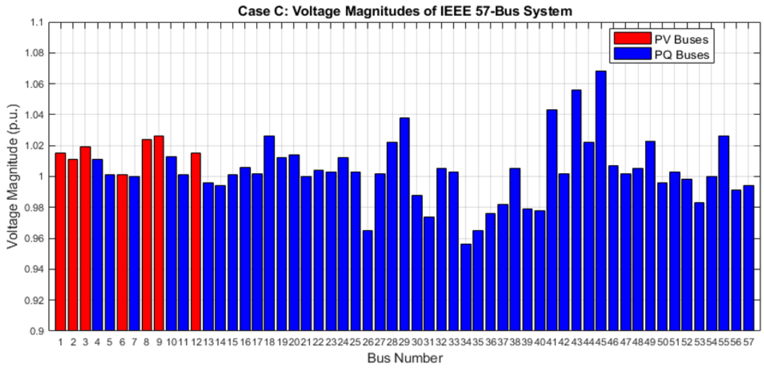

Figure 10. Voltage magnitudes of buses including PV and PQ buses for test case C.

Table 19. Configuration of modified IEEE 57 bus test system for case D.

Index	Components	Quantity	Configuration of components
1	Power generating units	7	At buses 1, 2, 3, 6, 8, 9 and 12
2	Transformers	15	Located at branches 19, 20, 31, 37, 41, 46, 54, 58, 59, 65, 66, 71, 73, 76 and 80
3	Branches	80	-
4	TCSC	4	Located at branches 13, 37, 57 and 61
5	SVC	4	At buses 23, 38, 39 and 48

Table 20. Operating limits of variables for case D.

Index	Variables	Lower limit	Upper limit
1	Generator bus voltages	0.95	1.1
3	Transformer's tap position settings	0.9	1.05
4	TCSC	0	0.11
5	SVC	0	0.20

Table 21. Active and reactive power flows as a result of load flow method to determine weak branches for case D.

Branch	From bus	To bus	From bus		To bus		Losses	
			Active power	Reactive power	Active power	Reactive power	Active power	Reactive power
13	13	14	-10.35	22.34	10.44	-23.10	0.087	0.29
37	24	26	-10.54	-1.55	10.54	1.61	-0.000	0.06
57	38	44	-24.35	5.23	24.52	-5.08	0.175	0.35
61	47	48	17.59	12.43	-17.51	-12.33	0.079	0.10

Table 22. Active and reactive power flows as a result of load flows after installing TCSC for case D.

Branch	From bus	To bus	From bus		To Bus		Losses	
			Active power	Reactive power	Active power	Reactive power	Active power	Reactive power
13	13	14	17.21	10.80	-17.15	-11.65	0.059	0.19
37	24	26	-3.57	0.79	3.59	-1.62	0.023	0.04
57	38	44	-14.75	2.59	14.82	-2.67	0.063	0.13
61	47	48	12.47	12.79	-12.42	-12.72	0.054	0.07

Table 23. VCPI based on weak bus voltages magnitude before and after installing SVC for case D.

Bus #	Before FACTS	After FACTS
4	0.981	1.006
20	0.964	0.977
22	1.010	1.015
28	0.997	1.033

The FMFO algorithm, with 20 particles, was applied to minimize power losses on the modified IEEE 57-bus system. Results for various fractional orders are listed in Table 24, while optimal SVC and TCSC placements are shown in Table 25. Figure 11 illustrates convergence over 500 iterations for q = 0.1 to 0.9. At q = 0.7, losses were 21.7914 MW with slow convergence. q= 0.9 improved speed but slightly increased losses to 21.8253 MW. At q = 0.6, losses dropped to 21.7779 MW with smoother behavior. Better performance appeared at q = 0.2 (21.6619 MW) and q = 0.1 (21.6362 MW). The best outcome was at q = 0.3, achieving 21.5911 MW with the most stable convergence. Table 26 compares these results with other methods such as coronavirus herd immunity optimizer (CHIO), EMFO-FPSO, FPSOGSA, FO-CLPSO, and others, showing that FMFO achieved the highest loss reduction of 22.5% from the base case of 27.86 MW. Compared to the base case value of 27.86 MW, the performance of the MFO technique led to a decrease of 12.95%, resulting in an objective value of 24.2529 MW. This suggests that fractional-order dynamics inclusion improves the performance of the optimization algorithm, leading to better reduction by FMFO compared to the MFO method. Control variable outputs from these methods are listed in Table 27. Bus voltage profiles for case D are depicted in Figure 12.

Table 24. Comparison of the proposed FMFO algorithm fractional orders (q=0.1 to 0.9) for test case D.

Variables	FMFO-1	FMFO-2	FMFO-3	FMFO-4	FMFO-5	FMFO-6	FMFO-7	FMFO-8	FMFO-9
V_{G1}	1.1000	1.1000	1.1000	1.1000	1.1000	1.1000	1.1000	1.1000	1.1000
V_{G2}	1.0991	1.0991	1.0992	1.0993	1.0993	1.0991	1.0990	1.0991	1.0991
V_{G3}	1.0885	1.0884	1.0887	1.0886	1.0886	1.0887	1.0889	1.0885	1.0888
V_{G6}	1.0835	1.0828	1.0834	1.0830	1.0835	1.0827	1.0838	1.0825	1.0836
V_{G8}	1.1000	1.1000	1.1000	1.1000	1.1000	1.1000	1.1000	1.1000	1.1000
V_{G9}	1.0855	1.0856	1.0857	1.0858	1.0858	1.0855	1.0860	1.0858	1.0850

Continued on next page

Variables	FMFO-1	FMFO-2	FMFO-3	FMFO-4	FMFO-5	FMFO-6	FMFO-7	FMFO-8	FMFO-9
V_{G12}	1.0816	1.0817	1.0819	1.0817	1.0824	1.0817	1.0817	1.0819	1.0812
T_1	0.9001	0.9001	0.9000	0.9108	0.9258	0.9089	1.0540	0.9371	1.0323
T_2	0.9000	0.9318	0.9000	0.9000	1.0111	0.9893	1.0211	1.0227	0.9140
T_3	0.9955	1.0178	0.9986	1.0119	1.0944	1.0448	1.1000	1.0998	1.0529
T_4	0.9833	0.9874	0.9857	0.9892	0.9900	0.9863	0.9793	0.9920	0.9822
T_5	0.9000	0.9000	0.9000	0.9000	0.9019	0.9000	0.9000	0.9000	0.9000
T_6	0.9775	0.9791	0.9792	0.9839	0.9976	0.9914	0.9975	0.9776	1.0091
T_7	0.9000	0.9000	0.9000	0.9000	0.9000	0.9000	0.9000	0.9000	0.9260
T_8	0.9000	0.9000	0.9000	0.9001	0.9000	0.9000	0.9032	0.9000	0.9000
T_9	0.9000	0.9000	0.9000	0.9000	0.9002	0.9000	0.9021	0.9000	0.9000
T_{10}	0.9130	0.9125	0.9129	0.9129	0.9128	0.9162	0.9189	0.9142	0.9139
T_{11}	0.9000	0.9000	0.9000	0.9000	0.9000	0.9000	0.9000	0.9000	0.9000
T_{12}	0.9002	0.9000	0.9000	0.9000	0.9007	0.9001	0.9421	0.9434	0.9203
T_{13}	1.0099	1.0237	1.0116	0.9928	1.0130	1.0267	0.9927	1.0652	1.0532
T_{14}	0.9820	0.9814	0.9806	0.9890	0.9802	0.9802	0.9778	1.0020	1.0385
T_{15}	0.9004	0.9014	0.9002	0.9014	0.9063	0.9033	0.9029	0.9026	0.9013
Q_{VAR18}	3.4591	4.0623	1.3052	0.6971	0.3090	0.1505	4.2468	0.9530	2.5573
Q_{VAR25}	4.9139	4.1577	5.0000	4.1319	0.5403	1.0090	3.2838	2.6548	3.8842
Q_{VAR53}	3.1592	3.3165	4.9332	2.5168	2.1500	4.6908	4.0949	2.1436	0.9791
Ploss (MW)	21.6362	21.6619	21.5911	21.6948	21.7165	21.7779	21.7914	21.8189	21.8253

Table 25. Optimum FACTS device placement and size for case D.

Optimal parameters	SVC-1	SVC-2	SVC-3	SVC-4	TCSC-1	TCSC-2	TCSC-3	TCSC-4
Location	23	38	39	48	13	37	57	61
Size	0.2	0.2	0.2	0.2	0.107	0.0242	0.071	0.11

Table 26. Comparative analysis of real power losses from the literature for test case D.

Algorithm	Ploss	Algorithm	Ploss	Algorithm	Ploss
CHIO [83]	24.3	GAEO [85]	23.25	ALO [82]	23.7834
EMFO-FPSO [39]	22.2663	SPSO [41]	22.1	EO [82]	21.6485
FPSOGSA [74]	27.21	APSO [41]	22.31	WOA [18]	21.8349
FO-CLPSO [40]	26.85	EPSO [41]	22.75	MPA [82]	21.6627
SOS [84]	23.36	LAPO [81]	22.6187	MFO [86]	24.2529

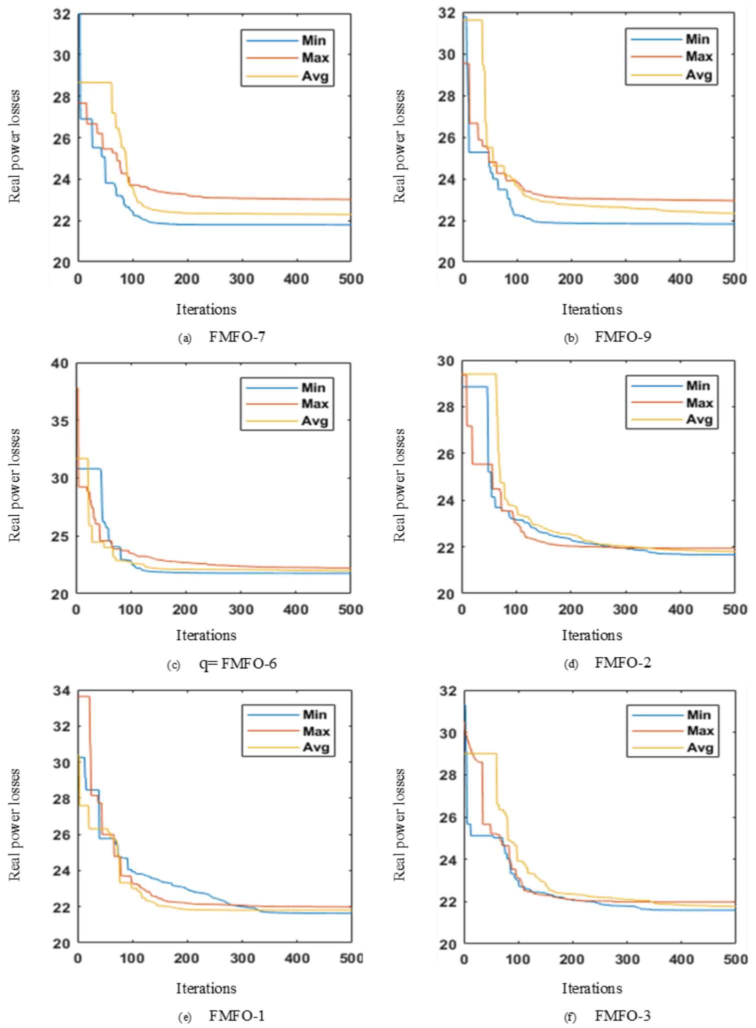

Figure 11. FMFO convergence curve of real power losses for case D at different fractional alpha orders.

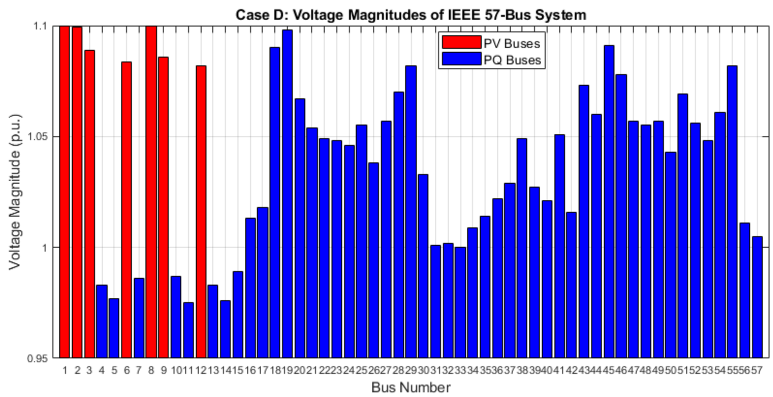

Figure 12. Voltage magnitudes of buses including PV and PQ buses for test case D.

Table 27. Outcomes of controlled variables utilizing several algorithms from the literature for test case D.

Controlled variables	Base case	MFO	FPSO-GSA	LAPO	MPA	CHIO	ALO	WOA	SOS	FMFO
V_{G1}	1.0400	1.0600	1.1000	1.0996	1.0999	1.09	1.09822	1.0999	1.0860	1.1000
V_{G2}	1.0110	1.0587	1.0987	1.0972	1.0921	1.046	1.0999	1.1	1.0847	1.0992
V_{G3}	0.9850	1.0469	1.0871	1.0988	1.09959	1.06	1.09989	1.0847	1.0709	1.0887
V_{G6}	0.9800	1.0421	1.0807	1.0871	1.0848	1.039	1.0361	1.07476	1.0558	1.0834
V_{G8}	1.0500	1.0600	1.1000	1.0986	1.0999	1.07	1.0879	1.09342	1.0789	1.1000
V_{G9}	0.9800	1.0423	1.0845	1.0937	1.09675	1.05	1.06392	1.04896	1.0483	1.0857
V_{G12}	1.0150	1.0373	0.9600	1.0933	1.08281	1.04	1.07609	1.07084	1.0551	1.0819
T_1	0.9700	0.9501	1.0071	1.0976	1.07337	0.95	1.05307	1.07708	0.9595	0.9000
T_2	0.9780	1.0076	1.0847	1.1	0.9535	0.92	1.0744	1.09964	1.0657	0.9000
T_3	1.0430	1.0063	0.9959	1.0645	1.0373	1	1.0555	1.09625	0.9373	0.9986
T_4	1.0430	1.0076	0.9908	1.0023	0.9997	0.98	1.09986	1.06297	0.9444	0.9857
T_5	0.9670	0.9752	0.9964	1.0777	0.9059	0.9	1.06461	0.94092	0.9441	0.9000
T_6	0.9650	0.9722	1.0072	0.9567	0.9282	1.03	1.01914	0.9436	0.9343	0.9792
T_7	0.9550	0.9000	0.9900	1.0944	0.9909	0.92	1.05934	0.90035	0.9926	0.9000
T_8	0.9550	0.9719	0.9906	1.0801	0.9242	0.9	1.02362	0.91404	0.9413	0.9000
T_9	0.9000	0.9536	1.0028	1.0778	0.9041	0.9	1.0545	0.9038	1.0468	0.9000
T_{10}	0.9300	0.9674	0.9900	1.0833	0.9037	0.91	1.0495	0.9018	0.9784	0.9129
T_{11}	0.8950	0.9279	1.0027	1.0844	0.9017	0.91	1.05070	0.90095	0.9866	0.9000
T_{12}	0.9580	0.9640	1.0844	1.0948	0.9062	0.9	1.09829	0.9629	0.9334	0.9000
T_{13}	0.9580	0.9998	1.0023	1.0622	1.0178	1	1.09953	1.05984	0.9688	1.0116
T_{14}	0.9800	0.9606	0.9900	0.9147	1.0244	1	1.07795	0.97769	0.9885	0.9806
T_{15}	0.9400	0.9789	1.0951	1.0932	0.9006	0.91	1.04607	0.94799	0.9555	0.9002
Q_{VAR18}	0	9.9968	4.9846	0.0108	1.9845	9	1.24469	3.68010	0.0542	1.3052
Q_{VAR25}	0	5.9000	4.9992	0.8726	1.999	5.5	1.36672	1.0933	0.0815	5.0000
Q_{VAR53}	0	6.3000	4.3653	1.4482	2.0067	5.4	2.02061	1.4355	0.0190	4.9332

5. Statistical analysis

This section presents a thorough statistical analysis that shows the consistent effects of the FMFO algorithm. A set of 100 independent trials are performed using the FMFO algorithm for case A using fractional order α=0.9 and case B using fractional order q=0.5 considering real power losses. Moreover, a set of 20 independent trials are performed for case C using fractional order q=0.9 and case D using fractional order q=0.9 considering voltage deviations and real power losses, respectively. The statistical evaluation is based on the least amount of fitness change over the course of each independent trial, histograms, the cumulative distribution function, and boxplots all of which are displayed in Figure 13, Figure 14, and Figure 15 for the standard IEEE 30 bus, modified IEEE 30 bus, standard IEEE 57 bus, and modified IEEE 57 bus test system respectively. The minimum fitness values across all test cases are shown in Figure 13(a), Figure 14(a), and Figure 15(a). The histograms shown in Figure 13(b), Figure 14(b), and Figure 15(b) demonstrate that most autonomous simulations of the FMFO provide the lowest values for the two fitness functions. The CDF probability plots are shown in Figure 13(c), Figure 14(c), and Figure 15(c). These plots demonstrate that in the event of independent trials, 80% of the real power losses are below 6.5 MW, 5 MW, and 21.9 MW for test cases A, B, and D, respectively. Furthermore, for test case C, 80% of the voltage deviations are below 0.75 p.u. The box plots in Figure 13(d), Figure 14(d), and Figure 15(d) indicate that the median of real power losses is approximately 5.4 MW, 5 MW, and 21.7 MW for case A, case B, and case D, respectively. Moreover, the box plot in Figure 15(d) indicates that the median voltage deviation is approximately 0.74 p.u for case C. In a nutshell, the ORPD case data show that the proposed FMFO algorithm is a substantial, and accurate optimization approach because of its stability, robustness, and consistency.

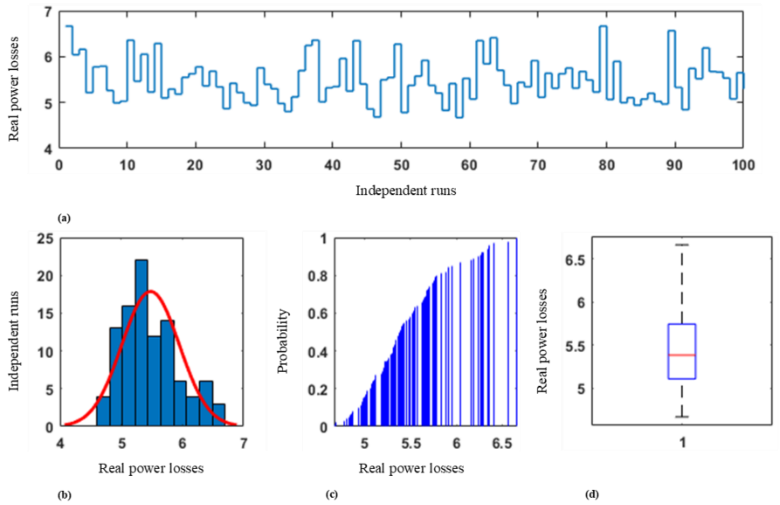

Figure 13. Case A statistical analysis for (a) real power losses minimization for 100 independent runs, (b) histogram, (c) CDF, and (d) boxplot analysis.

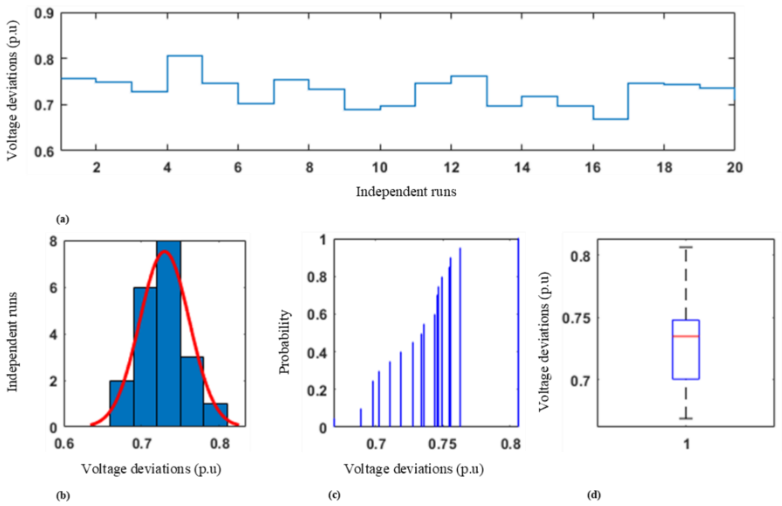

Figure 14. Case C statistical analysis for (a) voltage deviation minimization for 20 independent runs, (b) histogram, (c) CDF, and (d) boxplot.

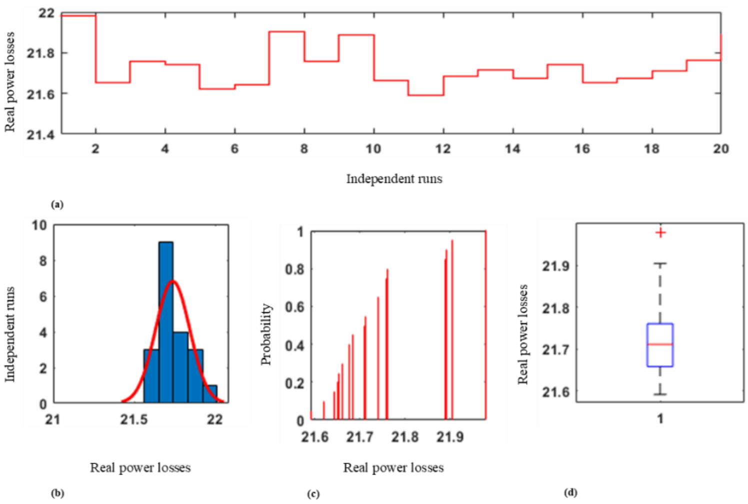

Figure 15. Case D statistical analysis for (a) real power losses minimization for 20 independent runs, (b) histogram, (c) CDF, and (d) boxplot analysis.

6. Conclusions and recommendations

The present research demonstrates significant advancements in power system optimization by using the proposed FMFO strategy. FMFO has notable efficacy in minimizing real power losses and voltage deviations. The adoption of the FMFO methodology resulted in significant enhancements in all four individual test cases. A comprehensive testing procedure was carried out on a number of different standard IEEE test systems in order to validate our proposed solution. Compared to conventional procedures, the outcomes show a noteworthy reduction in percentage of real power losses. In a modified IEEE 57 bus test system incorporating FACTS devices, the percentage loss drops to 22.5%, while in a modified IEEE 30 bus test system, it drops to 43.32%. Furthermore, a voltage deviation decreases of 84% was observed in the standard IEEE 57 bus test system. Despite its effectiveness, FMFO has some limitations. Its performance heavily depends on proper tuning of parameters. The lack of a clear mathematical foundation for fractional-order methods also makes them harder to apply than traditional algorithms. Moreover, their complexity in real-time use can affect reliability. Broader testing against standard methods is still needed to confirm their robustness across various scenarios. There are many possibilities for future research considering the promising results obtained by using FMFO:

1) Design self-adaptive techniques that will be capable of modifying inertia weight values, acceleration constants, and fractional-order components dynamically through the process of optimization.
2) Build a better mathematical theory that will enable one to study the convergence, stability, and dynamics of fractional-order swarm intelligence algorithms.
3) Explore parallel computation techniques, distributed computation techniques, and surrogate model methods for reducing computational burden and enhancing real-time usability.
4) Investigate the use of the FMFO algorithm along with machine learning approaches, and other reinforcement learning methods.

5) Test the performance of the algorithm in dealing with large-scale, highly constrained, and dynamic optimization problems.
6) Apply the proposed framework for solving optimization problems that consist of more than one objective and have conflicting objectives.
7) Applying FMFO to real-life challenges such as smart grid management, utilization of renewable energies, UAV navigation, robots, and industrial processing will serve as further validation of its efficacy.
8) Undertake comprehensive comparative analyses with respect to current state-of-the-art algorithms based on fractional order as well as traditional optimization techniques.
9) Design sophisticated constraint management techniques that can effectively handle non-linear and time-varying constraints in engineering systems.

Author contributions

Babar Sattar Khan: Conceptualization, Methodology, Software, Formal analysis, Writing-original draft; Affaq Qamar: Methodology, Software, Investigation, Data curation; Abdul Wadood: Conceptualization, Methodology, Formal analysis, Writing-original draft, Writing—review and editing, Visualization, Project administration; Hani Albalawi: Validation, Investigation, Writing-review and editing; Herie Park: Validation, Data curation, Visualization; Byung O Kang: Conceptualization, Writing-review and editing, Visualization, Supervision, Project administration. All authors have read and agreed to the published version of the manuscript.

Use of Generative-AI tools declaration

The authors declare they have not used Artificial Intelligence (AI) tools in the creation of this article.

Acknowledgments

This research was supported by Korea Electric Power Corporation (Grant number: R25XO03-14).

Conflict of interest

The authors declare no conflicts of interest.

References

1. A. Rajendran, K. Selvam, Multi-objective Chaotic-Enhanced Competitive Swarm Optimizer (CECSO) algorithm based optimal scheduling of microgrid with renewable energy sources, *Energy*, **334** (2025), 137550. https://doi.org/10.1016/j.energy.2025.137550
2. K. Y. Chan, K. F. C. Yiu, D. Kim, An Epsilon constraint-based evolutionary algorithm and multi-objective quality metrics for combined economic emission dispatch problem, *Neural Comput. Appl.*, **37** (2025), 17963–17992. https://doi.org/10.1007/s00521-025-11330-2

3. H. Tian, Y. Song, An augmented multi-objective multi-verse optimizer algorithm for solving dynamic economic emission dispatch problems, *J. Supercomput.*, **81** (2025), 1051. https://doi.org/10.1007/s11227-025-07527-w
4. S. B. Pandya, K. Kalita, P. Jangir, R. Cep, H. Migdady, J. S. Chohan, et al., Multi-objective RIME algorithm-based techno economic analysis for security constraints load dispatch and power flow including uncertainties model of hybrid power systems, *Energy Rep.*, **11** (2024), 4423–4451. https://doi.org/10.1016/j.egyr.2024.04.016
5. K. Nagarajan, A. Rajagopalan, M. Bajaj, V. Raju, V. Blazek, Enhanced wombat optimization algorithm for multi-objective optimal power flow in renewable energy and electric vehicle integrated systems, *Results Eng.*, **25** (2025), 103671. https://doi.org/10.1016/j.rineng.2024.103671
6. Y. A. Baysal, S. Ketenci, I. H. Altas, T. Kayikcioglu, Multi-objective symbiotic organism search algorithm for optimal feature selection in brain computer interfaces, *Expert Syst. Appl.*, **165** (2021), 113907. https://doi.org/10.1016/j.eswa.2020.113907
7. N. Khodadadi, E. Khodadadi, B. Abdollahzadeh, E. S. M. EI-Kenawy, P. Mardanpour, W. Zhao, et al., Multi-objective generalized normal distribution optimization: A novel algorithm for multi-objective problems, *Cluster Comput.*, **27** (2024), 10589–10631. https://doi.org/10.1007/s10586-024-04467-7
8. K. Kalita, N. Ganesh, R. Chandran Narayanan, P. Jangir, D. Oliva, Multi-objective water strider algorithm for complex structural optimization: a comprehensive performance analysis, *IEEE Access*, **12** (2024), 55157–55183. https://doi.org/10.1109/ACCESS.2024.3386560
9. S. Agrawal, S. Pandya, P. Jangir, K. Kalita, S. Chakraborty, A multi-objective thermal exchange optimization model for solving optimal power flow problems in hybrid power systems, *Decis. Anal. J.*, **8** (2023), 100299. https://doi.org/10.1016/j.dajour.2023.100299
10. P. Jangir, H. Buch, S. Mirjalili, P. Manoharan, MOMPA: Multi-objective marine predator algorithm for solving multi-objective optimization problems, *Evol. Intell.*, **16** (2023), 169–195. https://doi.org/10.1007/s12065-021-00649-z
11. M. Premkumar, P. Jangir, R. Sowmya, H. H. Alhelou, S. Mirjalili, B. S. Kumar, Multi-objective equilibrium optimizer: Framework and development for solving multi-objective optimization problems, *J. Comput. Des. Eng.*, **9** (2022), 24–50. https://doi.org/10.1093/jcde/qwab065
12. S. Mirjalili, S. Saremi, S. M. Mirjalili, L. D. S. Coelho, Multi-objective grey wolf optimizer: A novel algorithm for multi-criterion optimization, *Expert Syst. Appl.*, **47** (2016), 106–119. https://doi.org/10.1016/j.eswa.2015.10.039
13. M. N. Azghandi, A. A. Shojaei, H. Lotfi, Hybrid PSO-SFLA with fuzzy optimization for multi-area dynamic economic load dispatch and demand response, *Energy 360*, **3** (2025), 100021. https://doi.org/10.1016/j.energ.2025.100021
14. F. Tu, S. Zheng, K. Chen, Optimal active-reactive power dispatch for distribution network with carbon trading based on improved multi-objective equilibrium optimizer algorithm, *IEEE Access*, **13** (2025), 18899–18911. https://doi.org/10.1109/ACCESS.2025.3532750
15. A. Rajan, K. Jeevan, T. Malakar, Weighted elitism based Ant Lion Optimizer to solve optimum VAr planning problem, *Appl. Soft Comput.*, **55** (2017), 352–370. https://doi.org/10.1016/j.asoc.2017.02.010
16. W. S. Sakr, R. A. El-Sehiemy, A. M. Azmy, Adaptive differential evolution algorithm for efficient reactive power management, *Appl. Soft Comput.*, **53** (2017), 336–351. https://doi.org/10.1016/j.asoc.2017.01.004

17. B. Bhattacharyya, S. Kumar, Loadability enhancement with FACTS devices using gravitational search algorithm, *Int. J. Electr. Power Energy Syst.*, **78** (2016), 470–479. https://doi.org/10.1016/j.ijepes.2015.11.114
18. M. Badi, S. Mahapatra, B. Dey, S. Raj, A hybrid GWO-PSO technique for the solution of reactive power planning problem, *IJSIR*, **13** (2022), 1–30. https://doi.org/10.4018/IJSIR.2022010104
19. Y. Xue, Multi-strategy improved snake optimizer for library robot path planning problems, *J. Supercomput.*, **81** (2025), 1155. https://doi.org/10.1007/s11227-025-07570-7
20. F. Sun, Y. Xue, Enhanced sparrow search algorithm with whale optimization algorithm for feature selection, *Cluster Comput.*, **29** (2026), 81. https://doi.org/10.1007/s10586-025-05835-7
21. Y. Xue, F. Sun, Median-driven whale optimization algorithm with differential mutation for feature selection in students' reading habits, *J. Supercomput.*, **82** (2026), 86. https://doi.org/10.1007/s11227-025-08185-8
22. Z. Yan, H. Wen, Electricity theft detection based on extreme gradient boosting in AMI, *IEEE Trans. Instrum. Meas.*, **70** (2021), 1–9. https://doi.org/10.1109/TIM.2020.3048784
23. Y. Duan, Y. Zhao, J. Hu, An initialization-free distributed algorithm for dynamic economic dispatch problems in microgrid: Modeling, optimization and analysis, *Sustain. Energy Grids Netw.*, **34** (2023), 101004. https://doi.org/10.1016/j.segan.2023.101004
24. F. G. Montoya, R. Baños, C. Gil, A. Espín, A. Alcayde, J. Gómez, Minimization of voltage deviation and power losses in power networks using Pareto optimization methods, *Eng. Appl. Artif. Intell.*, **23** (2010), 695–703. https://doi.org/10.1016/j.engappai.2010.01.011
25. M. H. K. Tushar, C. Assi, Volt-VAR control through joint optimization of capacitor bank switching, renewable energy, and home appliances, *IEEE Trans. Smart Grid*, **9** (2017), 4077–4086. https://doi.org/10.1109/TSG.2017.2648509
26. C. A. Ordóñez, A. Gómez-Expósito, J. M. Maza-Ortega, Series compensation of transmission systems: A literature survey, *Energies*, **14** (2021), 1717. https://doi.org/10.3390/en14061717
27. S. Sayah, Modified differential evolution approach for practical optimal reactive power dispatch of hybrid AC–DC power systems, *Appl. Soft Comput.*, **73** (2018), 591–606. https://doi.org/10.1016/j.asoc.2018.08.038
28. E. Naderi, M. Pourakbari-Kasmaei, H. Abdi, An efficient particle swarm optimization algorithm to solve optimal power flow problem integrated with FACTS devices, *Appl. Soft Comput.*, **80** (2019), 243–262. https://doi.org/10.1016/j.asoc.2019.04.012
29. Y. Muhammad, R. Akhtar, R. Khan, Design of fractional evolutionary processing for reactive power planning with FACTS devices, *Sci. Rep.*, **11** (2021), 593. https://doi.org/10.1038/s41598-020-79838-2
30. M. Shirkhani, J. Tavoosi, S. Danyali, A. H. K. Sarvenoee, A. Abdali, A. Mohammadzadeh, et al., A review on microgrid decentralized energy/voltage control structures and methods, *Energy Rep.*, **10** (2023), 368–380. https://doi.org/10.1016/j.egyr.2023.06.022
31. Y. Zhou, Q. Zhai, Z. Xu, L. Wu, X. Guan, Multi-stage adaptive stochastic-robust scheduling method with affine decision policies for hydrogen-based multi-energy microgrid, *IEEE Trans. Smart Grid*, **15** (2023), 2738–2750. https://doi.org/10.1109/TSG.2023.3340727
32. S. Wang, T. Lu, R. Hao, J. Li, Y. Guo, X. He, et al., An identification method for anomaly types of active distribution network based on data mining, *IEEE Trans. Power Syst.*, **39** (2023), 5548–5560. https://doi.org/10.1109/TPWRS.2023.3288043
33. Y. Ju, W. Liu, Z. Zhang, R. Zhang, Distributed three-phase power flow for AC/DC hybrid networked microgrids considering converter limiting constraints, *IEEE Trans. Smart Grid*, **13** (2022), 1691–1708. https://doi.org/10.1109/TSG.2022.3140212

34. A. A. Abou El Ela, M. A. Abido, S. R. Spea, Differential evolution algorithm for optimal reactive power dispatch, *Electr. Power Syst. Res.*, **81** (2011), 458–464. https://doi.org/10.1016/j.epsr.2010.10.005
35. Y. Li, Y. Cao, Z. Liu, Y. Liu, Q. Jiang, Dynamic optimal reactive power dispatch based on parallel particle swarm optimization algorithm, *Comput. Math. Appl.*, **57** (2009), 1835–1842. https://doi.org/10.1016/j.camwa.2008.10.049
36. A. H. Khazali, M. Kalantar, Optimal reactive power dispatch based on harmony search algorithm, *Int. J. Electr. Power Energy Syst.*, **33** (2011), 684–692. https://doi.org/10.1016/j.ijepes.2010.11.018
37. M. Ghasemi, S. Ghavidel, M. M. Ghanbarian, A. Habibi, A new hybrid algorithm for optimal reactive power dispatch problem with discrete and continuous control variables, *Appl. Soft Comput.*, **22** (2014), 126–140. https://doi.org/10.1016/j.asoc.2014.05.006
38. B. Mandal, P. K. Roy, Optimal reactive power dispatch using quasi-oppositional teaching learning based optimization, *Int. J. Electr. Power Energy Syst.*, **53** (2013), 123–134. https://doi.org/10.1016/j.ijepes.2013.04.011
39. B. S. Khan, A. Qamar, F. Ullah, M. Bilal, Ingenuity of Shannon entropy-based fractional order hybrid swarming strategy to solve optimal power flows, *Chaos Solitons Fract.*, **170** (2023), 113312. https://doi.org/10.1016/j.chaos.2023.113312
40. Y. Muhammad, M. A. Z. Raja, M. Altaf, F. Ullah, N. I. Chaudhary, C. M. Shu, Design of fractional comprehensive learning PSO strategy for optimal power flow problems, *Appl. Soft Comput.*, **130** (2022), 109638. https://doi.org/10.1016/j.asoc.2022.109638
41. B. Bhattacharyya, S. Raj, Swarm intelligence based algorithms for reactive power planning with Flexible AC transmission system devices, *Int. J. Electr. Power Energy Syst.*, **78** (2016), 158–164. https://doi.org/10.1016/j.ijepes.2015.11.086
42. M. K. Kar, S. Kumar, A. K. Singh, S. Panigrahi, Reactive power management by using a modified differential evolution algorithm, *Optimal Control Appl. Meth.*, **44** (2023), 967–986. https://doi.org/10.1002/oca.2815
43. M. Mahato, A. Kumar, M. K. Singh, S. Sultana, S. Paul, S. Dutta, et al., Using the quasi-oppositional artificial hummingbird algorithm, a probabilistic optimal power flow for an integrated renewable power system comprising wind and solar, In: *2025 3rd International Conference on Intelligent Systems, Advanced Computing and Communication*, IEEE, 2025, 349–355. https://doi.org/10.1109/ISACC65211.2025.10969389
44. S. Mahapatra, S. Raj, Management of VAR sources for the reactive power planning problem by oppositional Harris Hawk optimizer, *J. Elect. Syst. Inf. Technol.*, **10** (2023), 45. https://doi.org/10.1186/s43067-023-00111-3
45. S. Mahapatra, N. Malik, S. Raj, M. K. Srinivasan, Constrained optimal power flow and optimal TCSC allocation using hybrid cuckoo search and ant lion optimizer, *Int. J. Syst. Assur. Eng. Manag.*, **13** (2022), 721–734. https://doi.org/10.1007/s13198-021-01334-1
46. S. Mahapatra, S. Raj, VAR strategic planning for reactive power using hybrid soft computing techniques, *Int. J. Bio-Inspired Comput.*, **20** (2022), 38–48. https://doi.org/10.1504/IJBIC.2022.126290
47. A. M. Abd-El Wahab, S. Kamel, M. H. Hassan, J. L. Domínguez-García, L. Nasrat, Jaya-AEO: An innovative hybrid optimizer for reactive power dispatch optimization in power systems, *Elect. Power Compon. Syst.*, **52** (2024), 509–531. https://doi.org/10.1080/15325008.2023.2227176

48. S. Jiao, C. Wang, R. Gao, Y. Li, Q. Zhang, A novel hybrid Harris Hawk sine cosine optimization algorithm for reactive power optimization problem, *J. Exp. Theor. Artif. Intell.*, **36** (2024), 901–937. https://doi.org/10.1080/0952813X.2022.2115144
49. M. S. Shaikh, S. Raj, R. Babu, S. Kumar, K. Sagrolikar, A hybrid moth–flame algorithm with particle swarm optimization with application in power transmission and distribution, *Decis. Anal. J.*, **6** (2023), 100182. https://doi.org/10.1016/j.dajour.2023.100182
50. K. Habib, A. Wadood, S. Khan, B. M. Khan, H. Park, B. O. Kang, et al., Enhancing variable frequency drive efficiency using fractional hybrid Particle Swarm Optimization and comprehensive thermal management, *Sci. Rep.*, **16** (2026), 11843. https://doi.org/10.1038/s41598-026-38644-y
51. A. Wadood, B. M. Khan, H. Albalawi, B. S. Khan, H. Park, B. O. Kang, Fractional calculus and adaptive balanced artificial protozoa optimizers for multi-distributed energy resources planning in smart distribution networks, *Fractal Fract.*, **10** (2026), 101. https://doi.org/10.3390/fractalfract10020101
52. A. Wadood, B. S. Khan, B. M. Khan, H. Park, B. O. Kang, A fractional hybrid strategy for reliable and cost-optimal economic dispatch in wind-integrated power systems, *Fractal Fract.*, **10** (2026), 64. https://doi.org/10.3390/fractalfract10010064
53. A. M. Alatwi, B. M. Khan, A. Wadood, S. Khan, H. M. El-Hageen, M. A. Mead, A fractional calculus-enhanced multi-objective AVOA for dynamic edge-server allocation in mobile edge computing, *Fractal Fract.*, **10** (2026), 28. https://doi.org/10.3390/fractalfract10010028
54. A. Wadood, H. Park, A novel application of fractional order derivative moth flame optimization algorithm for solving the problem of optimal coordination of directional overcurrent relays, *Fractal Fract.*, **8** (2024), 251. https://doi.org/10.3390/fractalfract8050251
55. A. Wadood, H. Albalawi, A. M. Alatwi, H. Anwar, T. Ali, Design of a novel fractional whale optimization-enhanced support vector regression (fwoa-svr) model for accurate solar energy forecasting, *Fractal Fract.*, **9** (2025), 35. https://doi.org/10.3390/fractalfract9010035
56. A. Wadood, A. F. Yousaf, A. M. Alatwi, An enhanced multiple unmanned aerial vehicle swarm formation control using a novel fractional swarming strategy approach, *Fractal Fract.*, **8** (2024), 334. https://doi.org/10.3390/fractalfract8060334
57. A. Wadood, E. Ahmed, S. Khan, H. Ali, Fraction order particle swarm optimization for parameter extraction of triple-diode photovoltaic models, *Eng. Res. Express*, **6** (2024), 025316. https://doi.org/10.1088/2631-8695/ad3f6f
58. N. Zhao, D. Lun, H. Zhang, X. Zhao, I. J. Rudas, Composite anti-disturbance control for networked systems with disturbances and actuator attacks via event-triggered output feedback, *IEEE Trans. Cybern.*, **56** (2026), 393–403. https://doi.org/10.1109/TCYB.2025.3609819
59. A. Wadood, H. Albalawi, S. Khan, B. M. Khan, A. M. Alatwi, Fractional-order african vulture optimization for optimal power flow and global engineering optimization, *Fractal Fract.*, **9** (2025), 825. https://doi.org/10.3390/fractalfract9120825
60. S. Mirjalili, Moth-flame optimization algorithm: A novel nature-inspired heuristic paradigm, *Knowl. Based Syst.*, **89** (2015), 228–249. https://doi.org/10.1016/j.knosys.2015.07.006
61. G. S. Teodoro, J. A. T. Machado, E. C. de Oliveira, A review of definitions of fractional derivatives and other operators, *J. Comput. Phys.*, **388** (2019), 195–208. https://doi.org/10.1016/j.jcp.2019.03.008
62. M. S. Couceiro, R. P. Rocha, N. M. F. Ferreira, J. A. T. Machado, Introducing the fractional-order Darwinian PSO, *Signal Image Video Process.*, **6** (2012), 343–350. https://doi.org/10.1007/s11760-012-0316-2

63. X. Yao, Y. Liu, G. Lin, Evolutionary programming made faster, *IEEE Trans. Evol. Comput.*, **3** (1999), 82–102. https://doi.org/10.1109/4235.771163
64. J. G. Digalakis, K. G. Margaritis, On benchmarking functions for genetic algorithms, *Int. J. Comput. Math.*, **77** (2001), 481–506. https://doi.org/10.1080/00207160108805080
65. M. Z. Naser, M. K. Al-Bashiti, A. T. G. Tapeh, A. Naser, V. Kodur, R. Hawileh, et al., A review of benchmark and test functions for global optimization algorithms and metaheuristics, *WIREs Comput. Stat.*, **17** (2025), e70028. https://doi.org/10.1002/wics.70028
66. R. Cheng, Y. Jin, M. Olhofer, B. Sendhoff, Test problems for large-scale multiobjective and many-objective optimization, *IEEE Trans. Cybern.*, 47 (2017), 4108–4121. https://doi.org/10.1109/TCYB.2016.2600577
67. H. Rezk, A. G. Olabi, M. Mahmoud, T. Wilberforce, E. T. Sayed, Metaheuristics and multi-criteria decision-making for renewable energy systems: Review, progress, bibliometric analysis, and contribution to the sustainable development pillars, *Ain Shams Eng. J.*, **15** (2024), 102883. https://doi.org/10.1016/j.asej.2024.102883
68. N. F. Johari, A. M. Zain, M. H. Noorfa, A. Udin, Firefly algorithm for optimization problem, *Appl. Mech. Mater.*, **421** (2013), 512–517. https://doi.org/10.4028/www.scientific.net/AMM.421.512
69. E. Cuevas, A. Echavarría, M. A. Ramírez-Ortegón, An optimization algorithm inspired by the States of Matter that improves the balance between exploration and exploitation, *Appl. Intell.*, **40** (2014), 256–272. https://doi.org/10.1007/s10489-013-0458-0
70. M. Abdel-Baset, I. Hezam, A hybrid flower pollination algorithm for engineering optimization problems, *Int. J. Comput. Appl.*, **140** (2016). https://doi.org/10.5120/ijca2016909119
71. X. S. Yang, Bat algorithm for multi-objective optimisation, *Int. J. Bio-Inspired Comput.*, **3** (2011), 267–274. https://doi.org/10.1504/IJBIC.2011.042259
72. E. Rashedi, H. Nezamabadi-Pour, S. Saryazdi, GSA: A gravitational search algorithm, *Inform. Sci.*, **179** (2009), 2232–2248. https://doi.org/10.1016/j.ins.2009.03.004
73. J. Kennedy, R. Eberhart, Particle swarm optimization, In: *Proceedings of ICNN'95–International Conference on Neural Networks*, **4** (1995), 1942–1948. https://doi.org/10.1109/ICNN.1995.488968
74. N. H. Khan, Y. Wang, D. Tian, M. A. Z. Raja, R. Jamal, Y. Muhammad, Design of fractional particle swarm optimization gravitational search algorithm for optimal reactive power dispatch problems, *IEEE Access*, **8** (2020), 146785–146806. https://doi.org/10.1109/ACCESS.2020.3014211
75. B. Bhattacharyya, V. K. Gupta, Fuzzy based evolutionary algorithm for reactive power optimization with FACTS devices, *Int. J. Elect. Power Energy Syst.*, **61** (2014), 39–47. https://doi.org/10.1016/j.ijepes.2014.03.008
76. S. Raj, B. Bhattacharyya, Optimal placement of TCSC and SVC for reactive power planning using Whale optimization algorithm, *Swarm Evolut. Comput.*, **40** (2018), 131–143. https://doi.org/10.1016/j.swevo.2017.12.008
77. R. Jamal, B. Men, N. H. Khan, M. A. Z. Raja, Y. Muhammad, Application of Shannon entropy implementation into a novel fractional particle swarm optimization gravitational search algorithm (FPSOGSA) for optimal reactive power dispatch problem, *IEEE Access*, **9** (2021), https://doi.org/10.1109/ACCESS.2020.3046317
78. M. Mehdinejad, B. Mohammadi-Ivatloo, R. Dadashzadeh-Bonab, K. Zare, Solution of optimal reactive power dispatch of power systems using hybrid particle swarm optimization and imperialist competitive algorithms, *Int. J. Elect. Power Energy Syst.*, **83** (2016), 104–116. https://doi.org/10.1016/j.ijepes.2016.03.039

79. K. Mahadevan, P. S. Kannan, Comprehensive learning particle swarm optimization for reactive power dispatch, *Appl. Soft Comput.*, **10** (2010), 641–652. https://doi.org/10.1016/j.asoc.2009.08.038
80. W. M. Villa-Acevedo, J. M. López-Lezama, J. A. Valencia-Velásquez, A novel constraint handling approach for the optimal reactive power dispatch problem, *Energies*, **11** (2018), 2352. https://doi.org/10.3390/en11092352
81. M. Ebeed, A. Ali, M. I. Mosaad, S. Kamel, An improved lightning attachment procedure optimizer for optimal reactive power dispatch with uncertainty in renewable energy resources, *IEEE Access*, **8** (2020), 168721–168731. https://doi.org/10.1109/ACCESS.2020.3022846
82. N. H. Khan, Y. Wang, D. Tian, R. Jamal, S. Iqbal, M. A. A. Saif, et al., A novel modified lightning attachment procedure optimization technique for optimal allocation of the FACTS devices in power systems, *IEEE Access*, **9** (2021), 47976–47997. https://doi.org/10.1109/ACCESS.2021.3059201
83. N. Rani, T. Malakar, A reactive power reserve constrained optimum reactive power dispatch using coronavirus herd immunity optimizer, *Elect. Power Compon. Syst.*, **50** (2022), 223–244. https://doi.org/10.1080/15325008.2022.2136287
84. Prasad, V. Mukherjee, R. P. Singh, Application of SOS algorithm for solution of ORPD problem, *J. Instit. Eng. (India): Ser. B*, **103** (2022), 747–766. https://doi.org/10.1007/s40031-021-00700-8
85. M. Hemeida, T. Senjyu, S. Alkhalaf, A. Fawzy, M. Ahmed, D. Osheba, Reactive power management based hybrid GAEO, *Sustainability*, **14** (2022), 6933. https://doi.org/10.3390/su14116933
86. R. N. Mei, M. H. Sulaiman, Z. Mustaffa, H. Daniyal, Optimal reactive power dispatch solution by loss minimization using moth-flame optimization technique, *Appl. Soft Comput.*, **59** (2017), 210–222. https://doi.org/10.1109/ITCE.2019.8646460